

AD-751 499

PROBLEMS ASSOCIATED WITH THE IMPROVEMENT
OF THE GASDYNAMIC LASER

Walter H. Christiansen

Washington University
Seattle, Washington

31 July 1972

DISTRIBUTED BY:

NTIS

**National Technical Information Service
U. S. DEPARTMENT OF COMMERCE
5285 Port Royal Road, Springfield Va. 22151**

**BEST
AVAILABLE COPY**

AD751499

12

Grant # DA-ARO-D-31-124-72-G8
Walter H. Christiansen

Problems Associated with the Improvement
of the Gasdynamic Laser

ANNUAL REPORT

Reproduced by
**NATIONAL TECHNICAL
INFORMATION SERVICE**
U S Department of Commerce
Springfield VA 22151

ARPA Order #675

Code # 62301D

U. S. Army Research Office, Durham

1 August 1971

31 July 1972

\$60,000

Washington Univ., Seattle
Aerospace Research Lab

388604

Grant # DA-ARO-D-31-124-72-G8

Walter H. Christiansen 206-543-6321

Problems Associated with the Improvement
of the Gasdynamic Laser

ANNUAL REPORT



I. INTRODUCTION

The development of the gasdynamic laser is one of the more important developments of the past decade. This laser, based on early works of Patel and others,^(1,2) obtains population inversion leading to laser action in CO₂ - N₂ mixtures by rapid expansion of the gases to supersonic speeds. Relatively high powers,⁽³⁾ 0(60Kw), in continuous wave operation have been achieved by this method, however, at very limited efficiency, 0(½ - 1%), based on radiated energy to flow enthalpy. It is the purpose of the current program to investigate methods for increasing this level of efficiency, the ideas of which may find application to other laser systems.

The main objective of the program is to utilize a larger fraction of the total enthalpy of the laser fluid for lasing action in an open cycle system. The most straight-forward way to accomplish this is to efficiently expand the gas, lase, recompress and repeat this process as many times as possible. The difficulties to this approach limit the viability of this idea and form the basis of our research; they are: (1) low radiated energy/flow energy which makes the cycle very sensitive to component inefficiency, (2) large entropy production during lasing in a channel, resulting in large loss of total pressure, and (3) difficulties during recompression (diffuser) stage with viscous effects that prevent efficient recompression.

Increasing the radiated energy/mass of fluid would solve problem area (1). Operation of a gasdynamic laser at higher temperatures would give this increased effect and accordingly during this contract period, our program investigated the basic kinetic processes of the laser mixture under high temperature conditions. Gain measurements of gasdynamic laser mixtures have been carried out at stagnation temperatures from 1700°K to 3700°K. Gain has been observed over this entire temperature range for low CO₂ concentration laser mixtures. Surprisingly though, our measurements show significantly higher gains than have been predicted over a wide range of conditions. It is believed that this apparent gain enhancement is possibly due to near resonant spectral line overlap of highly excited states. The results of the experimental gain study indicates that CO₂ - N₂ mixtures can be operated under high enthalpy conditions if a practical method of gas utilization at high temperatures can be found.

In addition we have just begun a numerical investigation of the lasing process using computer simulation. The primary aim is to thoroughly investigate the possibilities of reducing entropy production by lasing in an expanding flow rather than a constant area duct. The full system kinetics are being modeled (a four temperature and vibrational mode approach). One dimensional flow is assumed for simplicity, and an equivalent one dimensional radiation extraction process based on a laser amplifier approach is the preliminary program. Initial non-optimizer results tend to confirm early analytic predictions based on a model which ignored the complete kinetic processes.

As pointed out in the proposal, a completely supersonic laser cycle (nozzles as well as diffusers) may be a more efficient device over the more conventional de Laval nozzle (subsonic and supersonic, i.e. a mixed flow) system. It is hoped that avoiding transonic and subsonic flow in the diffuser will permit

a more efficient design than is currently possible while still carrying out the function of re-energizing the vibrational levels of the system. Part of the program is thus endeavoring to understand the non-ideal aerodynamics and kinetics of the all supersonic flow approach using the Prandtl Meyer turning vanes. Gain measurements in the Prandtl Meyer expansion flow have been completed. The measured gains were always somewhat lower than predicted, but this has been traced to insufficient testing time in the three-inch shock tube facility so that quasi-steady flow in the cavity region was not fully achieved. A boundary layer computer program incorporating the possibility of external pressure gradients and non-adiabatic walls is now beginning to give results. Preliminary outputs are now available to study their effect on diffuser performance.

These studies are individually explored in more detail in the following sections of the report.

II. HIGH ENTHALPY GAIN MEASUREMENTS

Most gasdynamic laser systems typically extract only $\frac{1}{2}$ - 1% of the total flow energy (enthalpy) as coherent radiation. One of the possible reasons for such low performance levels in GDL's is that low stagnation temperatures of from 1200°K to 1600°K are commonly used. At such low temperatures the vibrational energy levels of molecular nitrogen are not fully excited. Figure 1 illustrates the amount of energy/mole stored in the vibrational energy levels of N_2 as a function of temperature. The total vibrational energy increases steadily with temperature. While the vibrational energy in the first level reaches a maximum at about 5000°K, the total vibrational energy of the system greatly exceeds the energy stored in the first excited vibrational level above 2000°. This first vibrational level is the level that pumps the CO_2 molecule to its upper laser

level. The possibility of the upper vibrational levels cascading down to the first excited vibrational level of N_2 in a rapidly expanding nozzle flow would greatly enhance the pumping action of N_2 on the upper laser level of CO_2 and hence convert more of the flow energy of the gas into coherent radiation.

The use of high temperatures would increase the relaxation rate processes in rapidly expanding nozzle flow and hence hinder the freezing process that is necessary to obtain a population inversion in the nitrogen and in the upper laser level of CO_2 . Although nitrogen by itself is easily frozen, the amount of CO_2 in the mixture has a large effect on this freezing process and can adversely affect the attainment of a population inversion. However, through the use of starved CO_2 mixtures, the adverse effects of CO_2 on the freezing process can be significantly reduced.⁽⁴⁾ Such starved mixtures have proved very effective in GDL's using very high stagnation pressures ($p_0 \sim 100$ atm).⁽⁴⁾ Also at high temperatures, a $CO_2 - N_2$ gas mixture may effectively starve itself by dissociating the CO_2 . It is expected that the products of such a chemically dissociating flow (primarily CO , O , O_2 , NO) would have a smaller adverse effect on the freezing process than CO_2 . Thus, if the CO_2 can be kept dissociated during the early part of the expansion process, the freezing of the N_2 vibrational energy states will be greatly enhanced. Furthermore, the possibility of CO_2 being formed in the excited upper laser level upon recombination may add to the inversion.

With the above thoughts in mind, a series of gain measurements were undertaken to determine if any of the above effects of high stagnation temperatures would have a favorable effect on the performance of a GDL. The Aerospace Research Laboratory's 7" I.D. high pressure shock tube was used to drive a two dimensional supersonic nozzle. Gain measurements were made at about the Mach 5

station of the nozzle using three $\text{CO}_2 - \text{N}_2 - \text{He}$ gas mixtures containing approximately 10%, 5%, and 2.5% CO_2 . Stagnation temperatures were varied from 2000°K to 5000°K and stagnation pressure was kept constant at about 40 atms. The experimental results indicate that high temperature effects may indeed have a beneficial effect on the performance of a GDL. Detailed considerations of these effects are discussed further.

Experimental Apparatus and Technique

The general experimental technique used to measure gain was essentially that of Reference 4. A shock tube is used to produce a high pressure, high temperature $\text{CO}_2 - \text{N}_2 - \text{He}$ gas reservoir behind a reflected shock wave. The gas processed by the reflected shock is expanded through a de Laval nozzle producing a population inversion. Laser gain is then measured at the Mach 5 station of the nozzle. The shock tube is adequately described in Reference 4. The laser optical system and nozzle design were significantly changed from that of Reference 4 in an effort to increase the signal to noise ratio and to reduce damage to the nozzle blocks and germanium windows. Acoustic noise and mechanical vibrations and stress were severe for this series of tests.

The three gas mixtures used for these tests are as follows:

- (1) 10.73% CO_2 - 41.02% N_2 - 48.25% He
- (2) 5.18% CO_2 - 47.67% N_2 - 47.15% He
- (3) 2.63% CO_2 - 53.97% N_2 - 43.40% He .

These gas mixtures were obtained from Liquid Carbonic Corporation and are pure grade, i.e. 99.99% pure or better.

A sketch of the experimental apparatus is shown in Figure 2. The two dimensional nozzle blocks were machined from 304 stainless steel and mounted in an aluminum flange that mated with ARL's 7" I.D. high pressure shock tube. This

nozzle test station was designed to withstand impulse loaded pressures of 4000 psi. The nozzle had throat dimensions (h^*) of 0.1 cm high and 15.24 cm wide, a subsonic converging section with a 0.4 cm radius contour leading smoothly to the throat, and a supersonic diverging section with a half angle of about 15 degrees. The Mach 5 station was located 3.55 cm from the throat where the area ratio A/A^* was approximately 20. The total length of the nozzle was 5 cm. The combination germanium window mounts and "ears" were machined from brass and screwed into the nozzle flange until flush with the sides of the nozzle blocks. The ears were used to eliminate the effects of the shock tube recoil from disturbing the position of the laser probe beam with respect to the nozzle test station. The germanium windows were one inch in diameter and 1/8 inch thick and were held in position on the ends of the window mounts by 0.020 inch thick face plates. The windows were centered on the Mach 5 station of the nozzle and had a view dimension of one half inch in diameter.

The laser optical system was designed to substantially reduce noise feedback to the laser cavity. This noise feedback was produced by stray reflections from the optical parts of the nozzle test station (window and ears) that would vibrate during a test run. The noise feedback would be greatly amplified by the laser cavity and would prevent consistent and reliable gain measurements. To substantially reduce the feedback, the laser cavity was isolated from the nozzle optical parts by inserting a 10% transmitting beam splitter between the laser output and the nozzle. Thus, only 10% of the total laser output of 10 watts was utilized to make the gain measurements. The remaining laser output was dumped into a nearly perfect absorber of 10.6 μ laser radiation - a glass of water. Approximately 3% of the dumped beam was deflected by a beam splitter to an infrared detector that was used to monitor the laser output during a test run.

The laser gain measuring beam passed through the test station and into the gain measuring detector. A solenoid operated single sweep chopper was located on the laser side of the test station and was triggered to chop the beam after the useful test time was over. This provided a measure of the total laser output that was necessary to determine the gain. The chopper was necessary to eliminate uncertainty in the total laser output due to long time variations of the laser power and effects produced by loud acoustic and mechanical noise created by firing the shock tube that would disturb the laser output power. These acoustic and mechanical noises would typically reach the laser a few milliseconds after useful test time.

The gain detector and monitor detector voltage outputs and the stagnation pressure were recorded on oscillographs for each test run. The gain detector output was recorded on both a 1 msec/cm and 2 msec/cm time scale and a few mvolt/cm and 50 mvolt/cm voltage scales respectively. The stagnation pressure was recorded on the same oscillograph as the fast time scale gain measurement to correlate the gain detector output with the pressure history. The monitor detector output was recorded on the same oscillograph as the slow time scale gain detector output with a voltage scale of 5 mvolts/cm. Monitor detector output could then be compared directly with the gain detector output during a test run to determine the presence of any possible feedback. Thin film heat transfer gauges were used to measure the incident shock Mach number.

A typical test run is shown in Figures 3a and 3b for the 5.18% CO₂ gas mixture at a stagnation temperature of 2300°K and a pressure of 39.8 atm. In Figure 3a, the upper trace is the fast time scale gain trace and the lower trace is the stagnation pressure trace. The arrival of the incident shock and the sudden jump in pressure due to the reflected shock are clearly visible in

the pressure trace. The gain trace indicates a very short period of absorption ($< .1$ msec) as the nozzle flow gets started and then the production of positive gain as the flow is established at the nozzle Mach 5 station. The pressure drops $\frac{1}{2}$ msec after the reflected shock wave pressure rise due to the arrival of the shock tube driver expansion fan. The gain correspondingly goes down to zero or absorption.

In Figure 3b the upper trace is the slow time scale gain trace illustrating the gain signal described above and the chopping of the CO_2 gas laser probe signal by the single sweep chopper to determine the relative power of the laser probe signal with respect to the gain signal. The lower trace is the monitor detector and it indicates that virtually no feedback or noise affected the probe laser during the test run. The measured gain per meter for this particular test run was 0.55/meter.

Results and Discussion

The measured gain vs. stagnation temperature is shown in Figure 4. The temperature for each data point was calculated on the basis of the measured incident shock Mach number and equilibrium flow theory for a reflected shockwave without chemical reactions. The theoretical curves are based on the kinetic model and rate data as described in References 5 and 6. This kinetic model and rate data have been shown to be valid by experimental verification and comparison with other works (References 4 and 7) at temperatures below 2000°K .

The experimentally measured gain data agree with theory at 2000°K . At temperatures above 2000°K , the measured gain deviates considerably from the theory for the 2.63% and 5.18% CO_2 gas mixtures and only slightly for the 10.73% CO_2 mixture. A maximum in the measured gain occurs at about 2500°K for both the 2.63% and 5.18% CO_2 gas mixtures, the gain at these maxima being about 50% and

and 30% higher, respectively, than the theoretically predicted gain. Above 2500°K the measured gain gradually decreases but still remains considerably higher than theory. One test run (not shown on Figure 4) was performed with the 2.63% CO₂ gas mixture at a stagnation temperature of 5000°K which indicated zero gain. Possible mechanisms that could account for this difference between theory and experiment are discussed below.

Figure 5 is a plot of gain divided by CO₂ concentration vs. stagnation temperature. This plot shows that the principle of obtaining higher gain per CO₂ particle by using starved CO₂ gas mixtures is applicable for high temperatures as well as high pressures. At 2500°K the gain per particle for the 2.63% CO₂ mixture is over 4 times larger than the gain for the 10.73% mixture and 1.4 times larger than the 5.18% mixture. This increase in gain per CO₂ particle is brought about by the increased efficiency of the freezing process. The efficiency of the freezing process is characterized by the equation for gain.

$$g \sim \frac{N_{CO_2}}{N_{TOTAL}} (X_u - X_L)$$

where g = gain, N_{CO_2} = number density of CO₂, N_{TOTAL} = total number density of gas mixture, and X_u , X_L = fraction of CO₂ molecules in the upper and lower laser levels, respectively. We can write the mole fraction of CO₂ in the gas mixture as $\psi_{CO_2} = N_{CO_2}/N_{TOTAL}$ and hence obtain

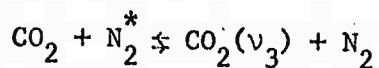
$$\frac{g}{\psi_{CO_2}} \sim (X_u - X_L) .$$

Thus we see that g/ψ_{CO_2} is a more direct measure of the population inversion than g is. The larger g/ψ_{CO_2} is, the larger the population inversion is, hence the more efficient the freezing process is. Energy storage of the gas mixture is also increased since a larger fraction of the CO₂ and N₂ is in the upper

excited state.

It is apparent from the plot of the data in Figure 4 that the mechanism that is producing the discrepancy between theory and experiment is very effective on the 2.63% and 5.18% CO₂ mixture but is rather ineffective on the 10.73% CO₂ gas mixture. Thus, the mechanism must display not only a temperature sensitivity, but also a very strong sensitivity to the concentration of CO₂. This sensitivity of the results to the concentration of CO₂ will prove to be the major stumbling block to any "simple" explanation of the discrepancy between theory and experiment.

Possible uncertainties in the rate data for the reaction



were looked into as a possible source of error in the theoretical predictions. The rate data for this reaction is not accurately known for temperatures near 2000°K.⁽⁵⁾ The rates were varied by as much as factors of 10 at high temperatures, but no consistent and reasonable results were obtained that matched the experimental data points.

The possible effects of the upper excited vibrational energy states of N₂ adding to the first vibrational energy state can be estimated on the basis of a simple calculation. Assuming equilibrium at the throat, we can calculate the number densities of the N₂ molecules in the various vibrational energy states at the throat. If we assume that all the nitrogen in the v = 2 excited state cascades down to the v = 1 state and remains frozen as the flow expands through the nozzle, we can recalculate the vibrational temperature of the N₂ molecules by simply adding the number density of these extra excited molecules to the number of v = 1 excited molecules as calculated from the regular theory. The following table shows the results for a stagnation temperature of 2500°K:

<u>Gas Mix</u>	<u>Regular Theory</u>		<u>Simple Addition</u> Process		<u>Experimental</u>
	T_{vib}	Gain	T_{vib}	Gain	Gain
10.73 CO ₂	1100	.36	1350	.70	.38
5.18 CO ₂	1500	.45	1740	.63	.58
2.65 CO ₂	1750	.31	2000	.40	.43

We see that the correction is reasonable for the 5.18% CO₂ mix, a little low for the 2.63% CO₂ mix, but completely wrong for the 10.73% mix. The 10.73% mix may deactivate the upper excited vibrational states faster which may make this simple calculation too high a correction. However, the calculation for the 2.63% CO₂ gas mixture would seem to indicate that the simple cascade process would have to be 100% efficient, a very unlikely result. Also this simple mechanism does not provide for a maximum gain at about 2500°K. It would seem unlikely that this process can account for the observed discrepancy between theory and experiment.

Dissociation effects can manifest themselves in three ways: (1) Chemistry effects behind the reflected shock wave will reduce the stagnation temperature for a given initial pressure and incident mach number, (2) dissociation of CO₂ may self starve the gas mixture during the early portion of the freezing process, (3) the energy of recombination may be dumped into the excited vibrational energy state of N₂.

To determine the effects of CO₂ dissociation on the stagnation temperature, chemical equilibrium calculations for a reflected shock wave were performed assuming the following seven chemical species were present, CO₂, N₂, He, CO, O₂, O, and NO. The chemical equilibrium temperature behind the reflected shock wave was calculated for a given p_1 , T_1 , and M_1 and compared to the no-chemistry calculations. The following table shows the results.

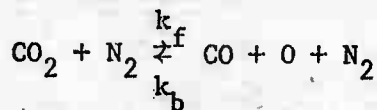
Gas Mix	T_o (no dissociation)	T_o (dissociation)	degree of dissociation
10.73% CO_2	2000	1980	.008
	2500	2430	.063
	3000	2750	.180
5.18% CO_2	2000	1990	.016
	2500	2430	.090
	3000	2830	.280
	3500	3160	.480
2.63% CO_2	2000	2000	.018
	2500	2490	.140
	3000	2890	.390
	3500	3270	.660

These results indicate no significant difference in the stagnation temperature @ 2000°K where the degree of dissociation of N_2 is very small. Above 2000°K, the T_o (dissociation) is lower than the T_o (no dissociation), the difference amounting to about 340°K at 3500°K for the 5.18% CO_2 mix. It should also be noted that the error in determining T_o is on the same order as the temperature correction. Correcting the experimental data on Figure 3 for the lower stagnation temperature would nicely correct the experimental results for the 10.73% CO_2 mix. However, it is obvious that lowering the temperature for the 2.63% and 5.18% CO_2 gas mixtures would not correct the data (except at the highest temperatures ~ 3500) as the measured gain between 2000°K and 3000°K lie entirely above the maximum theoretically predicted gain. Some other mechanism is affecting the gain for the two lower CO_2 gas mixtures. The effects of self starving is not expected to be of any importance due to the low degree of dissociation of the CO_2 , particularly at 2500°K where there is a maximum in the measured gain. If chemical equilibrium is assumed at the throat of the nozzle, the degree of dissociation drops by about

a factor of 4 and hence is even more insignificant as far as the self starving effect is concerned.

The amount of energy released in the recombination of CO and O to form CO₂ would have a significant effect on the gain if it were dumped into the first vibrational energy level of N₂, even though the degree of dissociation is very small. In order for the recombination process to add energy to the vibrational energy levels of N₂ in such a manner that the energy is frozen in these vibrational energy states, the relaxation time for recombination must be on the same order as or shorter than the vibrational relaxation time for N₂. Unfortunately, the following calculation will indicate that the recombination process is essentially frozen throughout the supersonic portion of the nozzle and hence cannot contribute any energy to the vibrational energy states.

Davis (8) has reported that the forward rate constant for the reaction



is given by

$$k_f = 4.07 \times 10^{-13} T^{1/2} \exp(0.23\text{eV}/kT) \text{ cm}^3 \text{ particle}^{-1} \text{ sec}^{-1}$$

The backward rate can be obtained by using the equilibrium constant for the above reaction. For the 5.18% CO₂ gas mix at a stagnation temperature of 2500°K at 40 atm, the equilibrium temperature at the throat is 2100°K at 21 atm. Chemical equilibrium calculations gives us the following number densities at the throat:

$$N_{\text{N}_2} = 3.5 \times 10^{19}$$

$$N_{\text{NO}} = 2.1 \times 10^{17}$$

$$N_{\text{CO}_2} = 3.7 \times 10^{18}$$

$$N_{\text{He}} = 5.5 \times 10^{19}$$

$$N_{\text{CO}} = 1.04 \times 10^{17}$$

$$N_{\text{O}_2} = 3.7 \times 10^{16}$$

$$N_{\text{O}} = 5.0 \times 10^{14}$$

The relaxation time for the recombination process is given by

$$\tau_{\text{rec}} \approx \frac{1}{k_b \frac{N_{\text{N}_2}}{N_{\text{O}}}} = 2.3 \text{ m sec}$$

An upper limit for the N_2 vibrational relaxation process can be obtained by considering a pure N_2 gas mix. From Millikan and White⁽⁶⁾ we obtain for 2100°K,

$$p\tau_{\text{vib}} \approx 500 \text{ atm } \mu\text{sec},$$

hence

$$\tau_{\text{vib}} \approx \frac{500}{21} = 24 \mu\text{sec}$$

Hence $\tau_{\text{rec}} \gg \tau_{\text{vib}}$ and it is unlikely that recombination in the supersonic portion of the nozzle will have any affect on the vibrational temperature of nitrogen.

Similar results were obtained for the other CO_2 gas mixtures.

If the energy of recombination is dumped into the vibrational energy level subsonically (the degree of dissociation varies from about 10% to 3% between the plenum and the throat) the vibrational temperature of N_2 will be higher at the throat than the translational temperature.

Calculations were performed using the regular theory to determine the effect on the gain of setting the N_2 vibrational temperature at the throat 500°K higher than the equilibrium temperature of 2100°K. These calculations indicated that the excess vibrational energy was quickly dumped back into translational energy and lower CO_2 vibrational energy levels by the relaxation collisions between CO_2 and N_2 . The net result was virtually no change in the predicted gain. Thus it is concluded that on the basis of the above precursory analysis dissociation has a negligible effect on the vibrational relaxation process and gain.

The contributions of other near resonance transitions may contribute significantly to the predicted gain. The predicted gain was calculated upon the

basis of the CO₂ vibration - vibration transition 001 → 100. Other near resonant transitions can be represented in general by

$$m, n, p+1 \rightarrow m+1, n, p$$

where $m = 0, 1, 2, \dots$, $p = 0, 1, 2, \dots$, and $n = 0, 1, 2, 3, \dots$. If we assume that these transitions are exactly resonant with the 001 → 100 transition we can calculate the maximum possible effect on the predicted gain.

The predicted gain for a given transition is proportional to the following:

$$g_{m,n,p} \propto \frac{1}{t_{m,p+1}} \left[\frac{N_{m,n,p+1}}{N} - \frac{N_{m+1,n,p}}{N} \right]$$

where N = total number of CO₂ molecules,

$N_{m,n,p+1}$ = number of CO₂ molecules in the $m,n,p+1$ state or upper laser level.

$N_{m+1,n,p}$ = number of CO₂ molecules in the lower laser level.

$t_{m,p+1}$ = lifetime of the upper laser level.

Based upon harmonic oscillator theory, we assume

$$t_{m,p+1} \propto \frac{1}{(m+1)(p+1)}$$

The total gain due to all possible transitions is given by

$$G = \sum_{m=0}^{\infty} \sum_{n=0}^{\infty} \sum_{p=0}^{\infty} g_{m,n,p}$$

Basov et al.⁹ gives for the quantity $N_{m,n,p}/N$ the following expression

$$\frac{N_{m,n,p}}{N} = [e^{-m\theta_1/T_1} (1-e^{-\theta_1/T_1})] [(n+1)e^{-n\theta_2/T_2} (1-e^{-\theta_2/T_2})^2] [e^{-p\theta_3/T_3} (1-e^{-\theta_3/T_3})]$$

where $\theta_1, \theta_2, \theta_3$ are the characteristic temperatures for the ν_1, ν_2, ν_3 vibrational modes of CO₂ (1920°K, 960°K, and 3380°K respectively), and T_1, T_2, T_3 are the effective vibrational temperatures for the modes ν_1, ν_2, ν_3 respectively.

Putting Basov's expression into the expression for the total gain and summing we obtain

$$G = [(1 - e^{-\theta_1/T_1}) (1 - e^{-\theta_2/T_2}) (1 - e^{-\theta_3/T_3})]^{-2} g_0$$

where g_0 = gain for the 001 \rightarrow 100 transition. This correction factor to the predicted gain g_0 is illustrated in figure 6 for the 2.63% CO_2 mixture. The temperatures T_1 and T_3 are the temperatures that the upper and lower laser levels (001 and 100 respectively) froze at as determined from the theory for predicting g_0 . The correction to the experimental data points from the lowering of the stagnation temperature due to dissociation effects are also illustrated. On the basis of a 4-temperature model for the kinetics of a CO_2 - N_2 -He gas mixture we assume $T_1 = T_2$.

The correction factor to the gain g_0 is about a factor of two larger than the experimentally measured gain. However, the correction factor does indicate a maximum at about 2500°K and the shape of the curve is in fair agreement with the experimental data. (This can be easily seen by lowering the curve for G such that $G = g_0$ at 2000°K).

Similar results were obtained for the 5.18% CO_2 gas mixture. Results for the 10.73% gas mixture indicated no maximum in the gain and the correction factor gave results that were only about 1.3 times larger than the experimental data. This latter results was primarily due to the smaller differences between T_1 and T_3 due to the faster relaxations effects for the 10.73% CO_2 mix. All of these results are in good qualitative agreement with the experimental data.

That the correction factor gives a gain that is too large is not surprising since exact resonance was assumed. The magnitude of the correction factor would be substantially reduced due to the fact that the various transitions are not exactly resonance. However, the general shape of the curve is expected to stay the same, i.e. showing a maximum at about 2500°K. Calculations performed by

Munjee and Christiansen (see appendix A) on the effects of pressure broadening of these near resonance lines on the absorption coefficient at 10.6μ indicates that the effect of these near resonance lines is typically $1/3$ as effective as an exact resonance would be. The results of reducing the difference between G and g_0 by a factor of $1/3$ (i.e. $\text{gain} = g_0 + 1/3(G - g_0)$) is also illustrated in figure 6. Although good agreement is obtained for $T_0 > 2500^\circ\text{K}$, the predicted gain is still too high for $T_0 < 2500^\circ\text{K}$. A maximum at about 2500°K is still indicated.

Qualitatively this near resonance effect appears to offer a very satisfactory explanation for the difference between the measured and predicted gain. More detailed calculations are in the process of being formulated and an experimental program involving changes in pressure as well as temperature is being set up to more firmly establish (or disprove) that this near resonance effect is indeed the mechanism that is responsible for the discrepancy between predicted and measured gain. The results of these investigations will be reported in the near future.

III. ENTROPY PRODUCTION DUE TO RADIATION EXTRACTION

Preliminary analysis⁽¹⁰⁾ of the thermodynamics of lasing a flowing media has shown that the normal dissipative effects and entropy production can be reduced ideally to zero. This analysis was based on a two temperature model at low concentration of CO_2 in which the upper laser level of CO_2 and the vibrational energy of N_2 could be characterized by a single temperature, T_v . The lower laser level, the lower vibrational states, and translational-rotational heat bath were characterized by another temperature T . For a one dimensional flowing gas with no collisional deactivation, it is easy to show that a small variation in entropy of the fluid during lasing is given by⁽¹⁰⁾

$$\delta s = \left[(1-\eta) \frac{T_v}{T} - 1 \right] \frac{\delta q_L}{\eta T_v} = \left[1 - (1-\eta) \frac{T_v}{T} \right] \delta s_v$$

where η is the quantum efficiency for CO_2 (0.4) and δs and δs_v are the variation in entropy of the system and vibrational states respectively, δq_L is the radiated energy. The requirement of gain in the laser system also stipulates that

$$T_v/T \geq \frac{1}{1-\eta} = 1.68$$

Thus for all $T_v/T > \frac{1}{1-\eta}$, it is seen that $\delta s > 0$, since $\delta s_v < 0$ when lasing occurs (for $T_v/T = \frac{1}{1-\eta}$ or zero gain, $\delta s = 0$). For T_v/T slightly greater than $\frac{1}{1-\eta}$, δs is only slightly greater than 0 and it can be shown that

$$\delta s = \frac{\delta e_v^2}{c T_v^2} = \frac{\delta q_L^2}{c \eta^2 T_v^2}$$

where $c = \frac{de_v}{dT_v}$ and δe_v is the variation in vibrational energy of N_2 . In this case entropy production is a higher order phenomena than laser energy out. Thus laser cavity systems with finite power extraction and no entropy production can be designed in principle. That is

$$\delta q_L \lim_{m \rightarrow 0} \frac{\Delta S}{\Delta Q_L} = \frac{\sum_{i=1}^m \delta s_i}{\sum_{i=1}^m \delta q_{L_i}} = \frac{1}{c T^2} \frac{\sum_{i=1}^m \delta q_{L_i}^2}{\sum_{i=1}^m \delta q_{L_i}} \gg 0$$

where ΔS and ΔQ_L are the net entropy change in the fluid and net finite laser energy output. To show this, let $\delta q_{L_i} = \delta q_L = \frac{\Delta Q}{m}$ as a constant differential energy output. Then the above equation becomes

$$\lim_{m \rightarrow \infty} \frac{\Delta S}{\Delta Q_L} = \frac{\delta q_L^2 m}{c T^2 \delta q_L m} = \frac{\Delta Q_L}{c T^2 m} \Rightarrow 0$$

In the limit of infinite number of steps, entropy production goes to zero with finite ΔQ_L .

To achieve this ideal result in practice requires that lasing takes place in a variable area channel such that T_v/T remains at all times close to the zero gain/meter value. For the case of T_v/T equal to a constant we have shown that the entropy of the fluid is related to the entropy change of the vibrational states by

$$\Delta S = [1 - (1-\eta)T_v/T] \left| \frac{\Delta S}{\text{const } T_v/T} \right.$$

Again we see that if $T_v/T = \frac{1}{1-\eta} = \text{const.}$, $\Delta S = 0$.

There are a number of questions to be asked concerning the validity of the simplified result for a CO_2 mixture before detailed examination of a cavity design can begin. Firstly, is mode analysis a valid approximation for CO_2 ? The general equations governing the transfer of energy between the vibrational mode of N_2 , the three modes of CO_2 , and translational-rotational bath are similar to those used in reference 9 with the addition of radiation terms. However, at high radiation intensities the energy transfer between modes is much more rapid than that due solely to collisional processes. Furthermore, radiation transfer usually occurs between two particular vibrational levels and not between modes. The validity of a mode analysis rests on the basic assumption that intramode V - V transitions are sufficiently rapid to ensure a Boltzmann distribution of levels at a characteristic mode temperature within each mode. This may not be valid at high radiation intensities and very low CO_2 concentrations. However while these probabilities are not precisely known it is believed that V - V energy transfer probabilities may be very large $0(\frac{1}{2})^{(11)}$ and therefore allow the use of mode analysis down to a level of CO_2 concentration of about 0.1%. Furthermore, some analysis by Yesil (Appendix B) shows that even if V - V rates are small or even ignored, it is difficult to get a very non-Boltzmann distribution of vibra-

ational states for time scales typical of GDL's. Therefore we feel mode analysis is a valid model.

Another important question to ask is how does the two temperature model compare with a more realistic 4-temperature model of Munjee⁽⁵⁾ and others (see also Appendix C) (T_{vN_2} , T_{v3CO_2} , $T_{v1} = T_{v2}$, T). One of the concerns is the effect of radiative saturation on entropy production. Unless intensities near saturation (defined as intensity required to reduce gain by two in presence of radiation) are used, the laser medium will be ineffective and collisional decay will result in a loss of vibrational energy and consequent increase of entropy. But if high intensity radiation is introduced to the system, then the mode temperatures are affected, also causing entropy production. Part of this problem also can be estimated by the following. The entropy of the fluid for a 4-temperature model is

$$\delta s = \frac{\delta e_{TR}}{T} + pdv + \frac{de_{vCO_2}}{T_2} + \frac{de_{vCO_2}}{T_3} + \frac{de_{vN}}{T_{vN}}$$

where de_{vCO_2}/T_2 is the contribution due to modes 1 and 2 of CO_2 , $\frac{de_{vCO_2}}{T_3}$ the entropy contribution due to mode 3 of CO_2 and $\frac{de_{vN}}{T_{vN}}$ the contribution of N_2 . If we specialize to low concentration of CO_2 , then the CO_2 contribution to the entropy of the system can be neglected, hence

$$\delta s \approx \frac{de_{TR} + pdv}{T} + \frac{de_{vN}}{T_{vN}}$$

From reference 10, this is still the same formula for the two temperature system and thus

$$\delta s = \left[(1-\eta) \frac{T_{vN}}{T} - 1 \right] \frac{dq_L}{\eta T_N} = \left[1 - (1-\eta) \frac{T_v}{T} \right] \delta s_v$$

Now in this case $T < T_2$ and $T_N > T_3$ (see e.g. 10) as the zero gain condition is $T_3/T_2 = \frac{1}{1-\eta} = 1.68$. Therefore $\delta s > 0$ under all cases and a net entropy is produced. We can readily see with the help of reference 12 that as a laser mixture is radiatively saturated $T \ll T_2$ and $T_N \gg T_3$ for large gain cases that a large entropy is produced. However for a low gain case T and T_N will be closer to T_2 and T_3 respectively and such large deviations will not be possible. Now the rate of power extraction is given by

$$dI/dx = gI \quad (\text{power/volume})$$

In the limit of very high intensities, the rate of power extracted is a maximum (for homogeneously broadened gain) and given by

$$\left. \frac{dI}{dx} \right|_{I \rightarrow \infty} = g_0 I_s$$

Since I_s does not depend on the vibrational energy of the system⁽¹²⁾ $dI/dx|_{I \rightarrow \infty}$ is a smaller rate for the low gain case (because g_0 is being deliberately kept near 0) than the high gain case. Thus in the presence of collisional deactivation of the laser states we have a compromise situation developing. By reducing the unsaturated gain toward zero we reduce the entropy production due to radiation extraction, but the rate of extraction is also reduced so that collisional decay becomes important. Thus the optimum in saturation is one which reduces gain only to a point where the net entropy generation is the smallest. Estimates show that the minimum value of g_0 is proportional to

$$g_0|_{\min} \sim \frac{\delta\tau_1 + \tau_4}{\tau_8} \neq \text{fn}(p)$$

where the coefficients are defined in reference 12. The basic relaxation times⁽⁶⁾ are sensitive functions of temperature and larger values of g_0 will be required at higher translational temperatures.

Some preliminary calculations using the computer simulation for various nozzle geometries are shown in the table below. In all the cases below, the medium was fully saturated, i.e. gain was kept at zero where lasing occurred.

EXAMPLE OF ENTROPY PRODUCTION DURING LASING

Basic Conditions

Concentrations: 1% CO₂, 60% N₂, 39% He

p_o = 100 atm

T_o = 1500°K

I → ∞ for g_o = 0⁺

Throat height, h* = 0.1 cm

	<u>Nozzle Description</u>	<u>Δe_v</u>	<u>ΔS/R</u>
CASE 1	20° half angle wedge to A/A* = 10, Lase at constant area channel	12.9 J/gm	.079
CASE 2	20° half angle wedge to g _o = 0 10° to A/A* = 4.1 5° to A/A* = 6.2 2° to A/A* = 23	12.7 J/gm	.068
CASE 3	20° half angle wedge to g _o = 0 6° to A/A* = 3.6 3° to A/A* = 5.1 1° to A/A* = 13	12.9 J/gm	.052

Case 1 represents a standard case whereby lasing takes place in a constant area channel where the Mach number is about 4. During the lasing phase there is about an 8% increase in entropy for an energy extraction of 5.9 KJ/# (12.9 J/gm). However by contouring the nozzle differently during the power extraction phase, as in Cases 2 and 3, an improvement is possible for the same energy out/gram. The best case is number 3 where there is only about 5% of an entropy increase. This is not as good as we would like and it certainly does not represent an optimum situation. The results do reflect the effect of collisional deactivation of the

upper laser level and the 4-temperature model. We are looking into numerical procedures whereby the optimum nozzle geometry can be calculated by the computer.

IV. NEW NOZZLES AND NOZZLE-DIFFUSER COMBINATIONS

The Supersonic Nozzle

A way of accomplishing the rapid increase in flow cross-sectional area required for an all supersonic gasdynamic laser is shown schematically on figure 7. Here an incoming supersonic stream is turned and expanded through an array of simple Prandtl - Meyer expansion fans. One side of each nozzle element consists of a sharp corner, while the other is contoured to cancel the incident expansion wave. Due to the fact that all of the high velocity incoming flow is directly expanded, a high mass flux and power are expected for a given pressure capability. This feature makes the supersonic turning nozzle particularly attractive for shock tube applications. (13)

The kinetic performance of these nozzles has been compared with conventional convergent-divergent nozzles. (14) A two temperature model was used for the N_2-CO_2 system, and the calculations were carried along separate streamlines in order to find average exit properties. It was found that an individual supersonic nozzle will produce less power per unit of mass flux, (χ) , for the same mixture, expansion area ratio, total temperature (T_0), and product of total pressure (p_0) times throat height (h). The difference is primarily due to the lower entering vibrational temperature for the high speed case. χ is given by

$$\chi = 0.4[e_v(T_v) - e_v(1.68T)]_{N_2}$$

where the vibrational energy, e_v , is evaluated for a particular N_2 concentration, T_v is the vibrational temperature, and T is the translational-rotational temperature of the expanded flow. T_v and T are known for perfect freezing ($p_0 h = 0$), and the above parameter can be evaluated for the nozzle configuration being considered.

As a first approximation the ratio of this parameter at $p_o h = 0$ can be used to predict relative performance at finite $p_o h$. More precise calculation requires the use of the two temperature model calculations, ⁽¹⁴⁾ or even better, the four temperature program of Appendix C. The χ reduction for an individual supersonic nozzle could be easily overcome by a decrease in relative $p_o h$ (the supersonic nozzles operate in a lower pressure environment and are stronger), an increase in the expansion area ratio, or by a direct increase in T_o . As will be discussed, the supersonic nozzles appear to be more suitable for staging purposes because of the relatively low p_o losses. Further, the power from a single stage is considerably greater for the turning nozzle because the number of nozzle elements that can be fitted onto a given duct is increased directly as the nozzle area ratio.

A grid of supersonic turning nozzles has been constructed, consisting of twenty $h = 1$ mm elements which together expand a 2×5 cm flow to 20×5 -cm. The array is fed through a sharp-edged rectangular pipe by a 7.5 cm shock tube. Using an external CO_2 laser, gain has now been measured in the expanded flow. ⁽¹⁵⁾ It has been found necessary to shorten the inlet pipe and use the two extreme nozzles as boundary layer bleeds. This stopped choking of the end nozzles and consequent propagation of shock waves across the cavity flow. A sample gain trace is shown on figure 7 for a run with the boundary layer bleeds installed. A mixture of 40% N_2 , 10% CO_2 , and 50% He by volume was used, with the shock tube operated so as to produce $T_o = 2100^\circ K$, $p_o h = 1.0$ atm cm, and an inlet Mach number of ≈ 1.5 . Absorption is first observed as the incident shock begins to cut across the beam axis. From earlier aerodynamic studies ⁽¹⁶⁾, a rearward facing starting shock is expected to follow and initiate the lasing flow. This wave begins to cross the beam axis after $\approx 200\mu sec$ and the absorption decreases as the nonequi-

librium gas appears. The lower trace on the figure was obtained with a pressure gage mounted in the cavity wall and more clearly shows the passage of the two shock waves. The second or starting shock is slow to form and move out of the cavity, and little if any plateau is reached in the gain trace before the flow begins to be cut off by the arrival of the shock tube driver gas. The gain climbs near to the calculated level, but the experiment is not definitive. As calculations show that lengthening the shock tube will not substantially increase the test time, a conversion to combusted Ludwig tube operation is being carried out.

Staging

It was mentioned in the Introduction that nozzle arrays can be staged so as to increase χ if sufficient pressure ratio is available. As a first approximation to a staged system, assume that $p_0 h$ is kept constant for each stage by increasing the nozzle dimension as p_0 falls. Assume also that the laser energy extracted is a small fraction of the total enthalpy so that T_0 is essentially exchanged. If λ is the p_0 entering a stage divided by that recovered at the diffuser exit, then

$$\lambda^n = p_{oi}/p_{oe}$$

where n is the number of stages that can be accommodated between the total pressure entering the first stage (p_{oi}), and that exiting the last stage (p_{oe}). The specific power of a staged system, χ_s is then given by χ times n or

$$\chi_s = (\chi/\ln\lambda) \ln p_{oi}/p_{oe}$$

where χ is the specific output per stage. The performance of a staged system thus depends on p_{oi}/p_{oe} and $\chi/\ln\lambda$, the latter being a staging figure of merit.

It was just pointed out that χ is reduced for the all supersonic nozzle. The nonequilibrium p_0 loss would also be reduced, but more importantly,

substantial reductions in diffuser losses are expected. The losses are discussed in the following sections, which consider two all-supersonic configurations. In the first, a single large diffuser is used to recompress the flow prior to expansion in a subsequent turning nozzle array. In the second case, a diffuser is machined as an upstream integral part of each nozzle element. In this idealized case it is no longer necessary to turn the flow in the supersonic expansion, and a laser cavity would follow each array of diffuser-nozzles fitted to a straight duct.

Gaskinetic Losses in Nozzle Diffuser Systems

The nonequilibrium losses have been calculated for representative nozzle diffuser combinations using both a two-temperature and a four-temperature (Appendix C) model for the $N_2 - CO_2$ system. Figure 8 is an example of the latter procedure applied to the centerline of a simple symmetric supersonic configuration. The flow expands from $M = 1.3$ through a 15° half-angle wedge nozzle to a lasing channel which has ten times the cross-sectional area of the nozzle throat and a length of over 200 throat heights. A 7° wedge diffuser then recompresses the flow back to equilibrium at $M = 1.3$ prior to subsequent re-expansion and laser energy extraction. The figure is for a 40% N_2 , 10% CO_2 , and 50% He mixture at $T_0 = 2000^\circ K$, with $p_0 h = 1$ atm cm. T_N denotes the N_2 vibrational temperature, T_U and T_L the upper and lower vibrational levels of CO_2 respectively, and T the translational-rotational temperature. All four temperatures are seen to approach each other in the diffuser, however the lag in T_U and T_N is such that an extended throat region (1-2 throat heights long) will generally be required. The specific entropy production rate (ds/dx) may be found using the relation

$$ds = \frac{de_N}{T_N} + \frac{de_U}{T_U} + \frac{de_L}{T_L} + \frac{dQ}{T},$$

where $dQ = -(de_N + de_U + de_L + de_{LASE})$. Here de_N , de_U , and de_L represent the increase in the various vibrational energy storages per unit mass of mixture, with dQ being the change in translational-rotational energy and de_{LASE} the energy removed by lasing. The lower part of Figure 8 shows that the entropy for this particular flow was about equally produced in the initial nonequilibrium expansion and in the lasing channel, with a smaller contribution from the diffuser. Neglecting changes in T_0 , the ratio of p_0 between exit and entrance equilibrium states is found from the total entropy change to be ~ 0.80 .

As discussed in Section III, use of a carefully shaped combination nozzle and lasing channel can reduce losses of the total pressure. Larger scale diffusers would accomplish equilibration near the entrance region with a further reduction in loss. While it is not geometrically possible to use such diffusers with symmetric supersonic nozzle elements (such as Figure 7), their use with supersonic turning nozzled could reduce the diffuser p_0 loss due to flow nonequilibrium to 1-2%. The calculations show that with advanced nozzle contours, large diffusers, and optimized running conditions, it should be possible to build supersonic configurations with less than 10% nonequilibrium p_0 loss without significant change in χ .

Fluid Mechanical Losses

Fluid mechanical loss calculations have been carried out for a representative series of diffuser-nozzle combinations. Air was used for the working fluid, with $T_0 = 2000$ K, $p_0 h = 1$ atm cm, and $h = 0.1$ cm. The normal cavity Mach number was 4. This flow is fed into a 2-D diffuser (area ratio = 10, half-angle = 7°), followed by a 0.1 cm long throat and a 15° half-angle nozzle.

The system of oblique shocks in the wedge diffuser produced a calculated p_0 loss of $\approx 10\%$. The boundary layer was assumed to undergo transition at the

first shock boundary layer interaction. An integral analysis was used up to this point, followed by the turbulent boundary layer procedure of Sasman and Cresci.⁽¹⁷⁾ The latter was initiated with the assumption that the momentum thickness (θ) was preserved across the interaction. Values of the dimensionless displacement thickness (δ^*/h) equal to ≈ 1.0 and $\theta/h \approx 0.5$ were obtained at the nozzle exit after carrying the calculation through the individual diffuser-nozzle channel. When mixed at constant area, this produced a p_o loss of 48%.

Much smaller losses were found when the diffuser scale was increased by two orders-of-magnitude. In this configuration, a single large diffuser would feed an array of turning nozzles. The diffuser exit boundary layer accounted for only $\approx 7\%$ of the mass flux and could be bled off, directly reducing χ . The individual nozzle boundary layers now start and develop in a favorable pressure gradient, and both analysis and experiment show them to be laminar. Exit thicknesses are now found to be $\delta^*/h \approx 0.8$ and $\theta/h \approx 0.03$, resulting in a mixing loss of 15% in p_o .

Including a representative nonequilibrium loss of 10% in p_o , the collected effects lead to a staging figure of merit $\chi/\ln(p_{oi}/p_{oe})$ of 40J/gm for the turning nozzle configuration. This is over twice that for the combination diffuser-nozzle elements, and is considerably larger than that obtainable with conventional supersonic-to-subsonic diffusers and nozzles. Further, it is probable that the boundary layer will relaminarize in the small diffuser case due to the high acceleration in the throat region.⁽¹⁸⁾ This has been indirectly observed in laboratory experiments, and it should make the losses quite similar for the two supersonic cases studied. Boundary layer control through bleed, mass injection, and wall cooling are being studied. The diffuser must have a turbulent boundary layer in order to remain attached; however, it should be

possible to reduce the shock losses with use of contoured walls, at least in the large scale case. The practical problem of diffuser starting⁽¹⁹⁾ is also being considered.

REFERENCES

1. C.K.N. Patel, Phys. Rev. Letters 13, 617 (1964).
2. I.R. Hurle and A. Hertzberg, The Phys. of Fluids 8, 1601 (1965).
3. E.T. Gerry, IEEE Spectrum 7, 51 (1970).
4. W.H. Christiansen and G.A. Tsongas, The Phys. of Fluids 14, 2611 (1971).
5. S.A. Munjee, The Phys. of Fluids 15, 506 (1972).
6. R.L. Taylor and S. Bitterman, Rev. Mod. Phys. 41, 26 (1969).
7. J.D. Anderson, R.P. Humphrey, J.S. Vamos, M.J. Plummer and R.E. Jensen, The Phys. of Fluids 14, 2620 (1971).
8. W.O. Davies, J. Chem. Phys. 41, 1846 (1964).
9. A. Basov, et al., Sov. Phys.-Tech. Phys. 13, 1630 (1969).
10. A. Hertzberg, W.H. Christiansen, E.W. Johnston and H.G. Ahlstrom, AIAA J. 10, 394 (1972).
11. Private communication with C.B. Moore, University of California, 1972.
12. A.L. Hoffman and G.C. Vlases, J. Quant. Elect. QE-8, 46 (1972).
13. D.A. Russell, W.H. Christiansen and A. Hertzberg, Proceedings VIII Int'l Shock Tube Symp.; ed. J.L. Stollery, A.G. Gaydon and P.R. Owen, Chapman and Hall, London (1971).
14. D.A. Russell, R.A. Tennant and G.W. Butler, Air Force Sys. Command Tech. Rpt. AFWL-TR-71-15 (March 1971).
15. D.A. Russell, G.S. Knoke and R.A. Tennant, Bull. Amer. Phys. Soc. 16, 11, 1332 (1971).
16. S. Byron, et al., Air Force Sys. Command Rpt., AFWL-TR-70-151 (Feb. 1971).
17. P.K. Sasman and R.J. Cresci, AIAA J. 4, 19-25 (Jan. 1966).
18. J.L. Nash-Weber and G.C. Oates, ASME paper 72-FE-19 (March 1972).
19. T. Jones and S. Neice, Math. Sci. NW Report 71-66-4, prepared for Air Force Sys. Command, Kirtland Air Force Base, NM (June 1971).

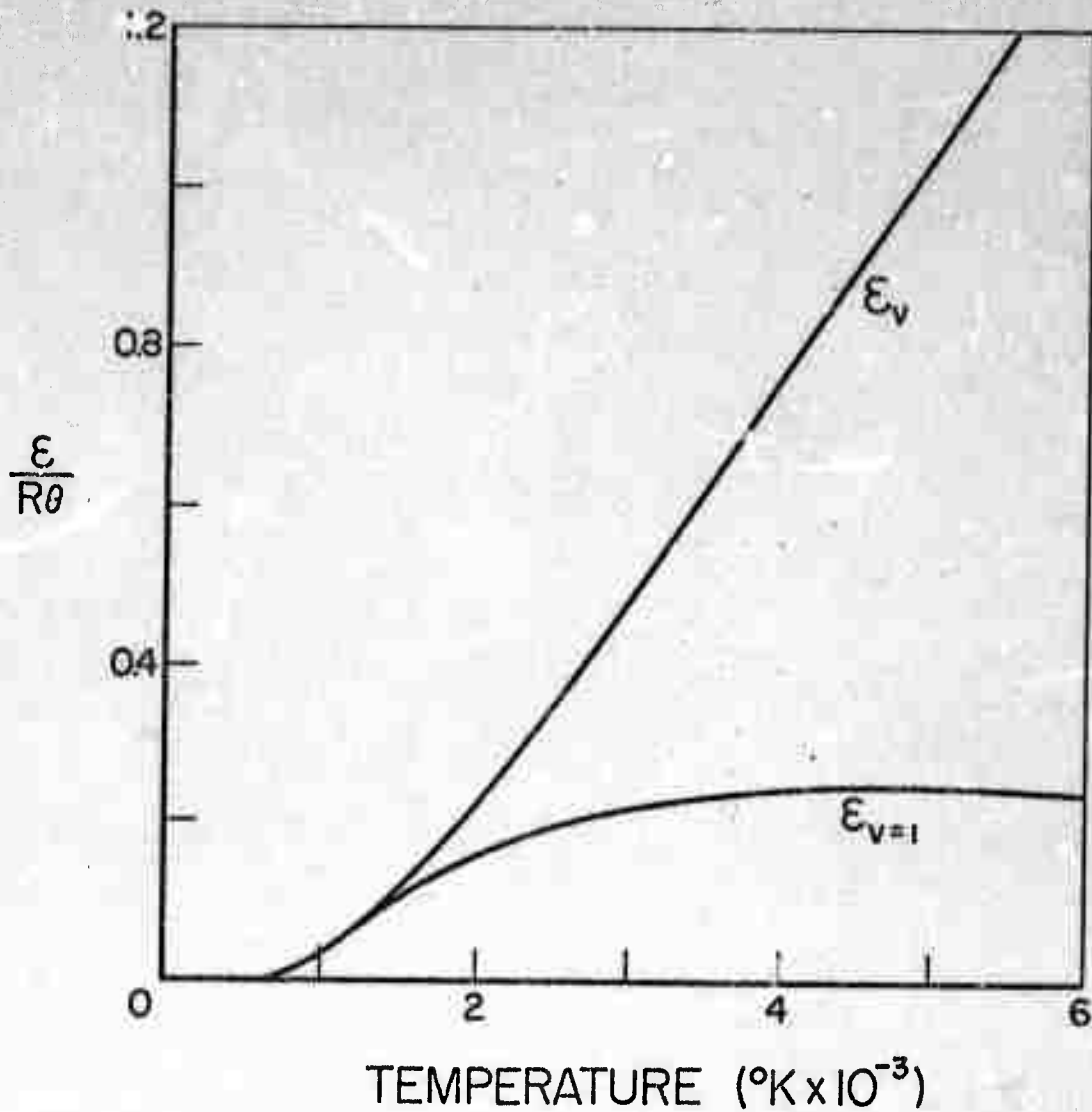


Figure 1. Vibrational energy/mole in N_2 normalized by the characteristic energy of the first level $R\theta$ ($\theta = 3350^\circ K$). E_v represents the total vibrational energy while $E_{v=1}$ represents only the first vibrational level.

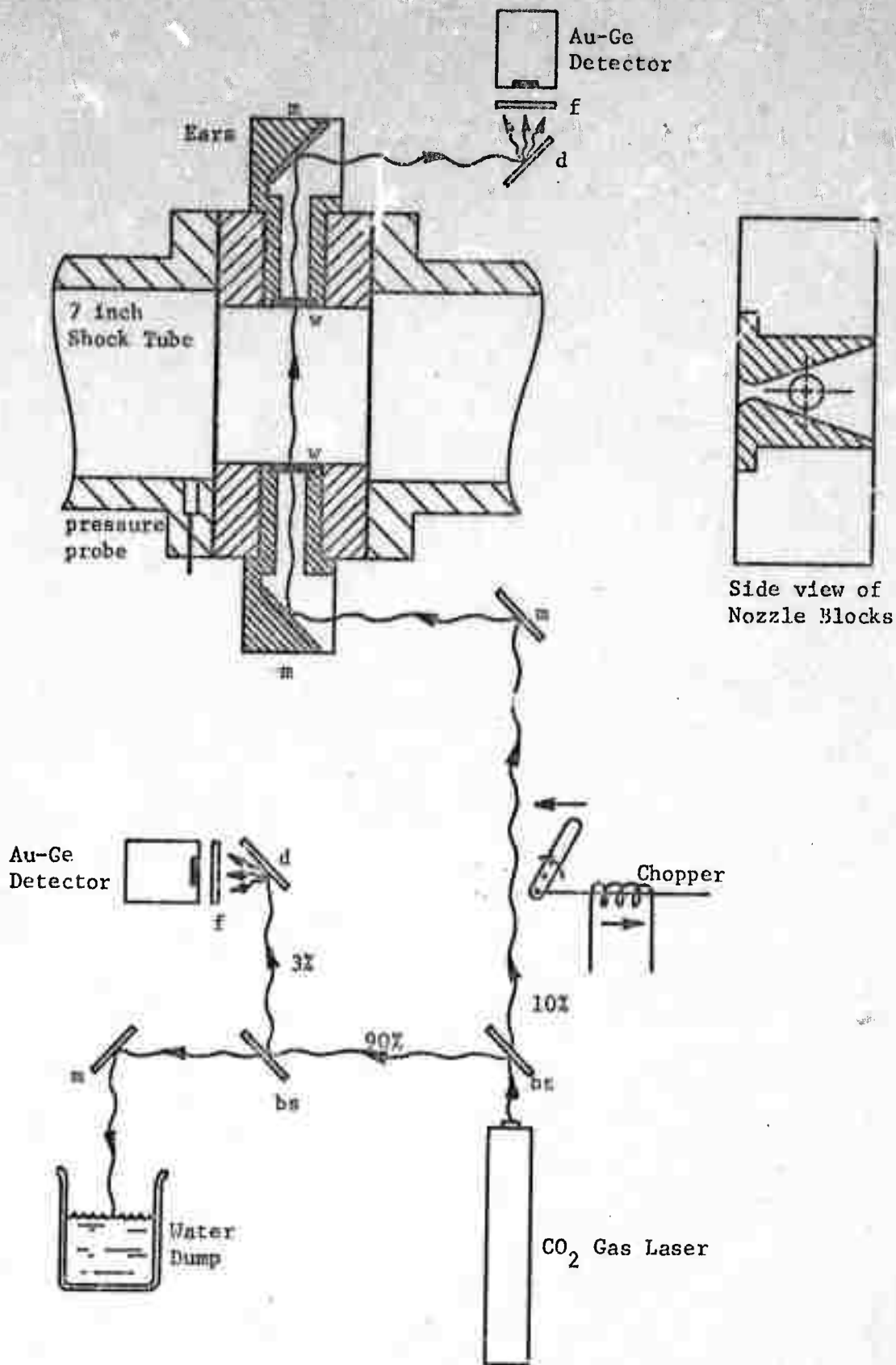
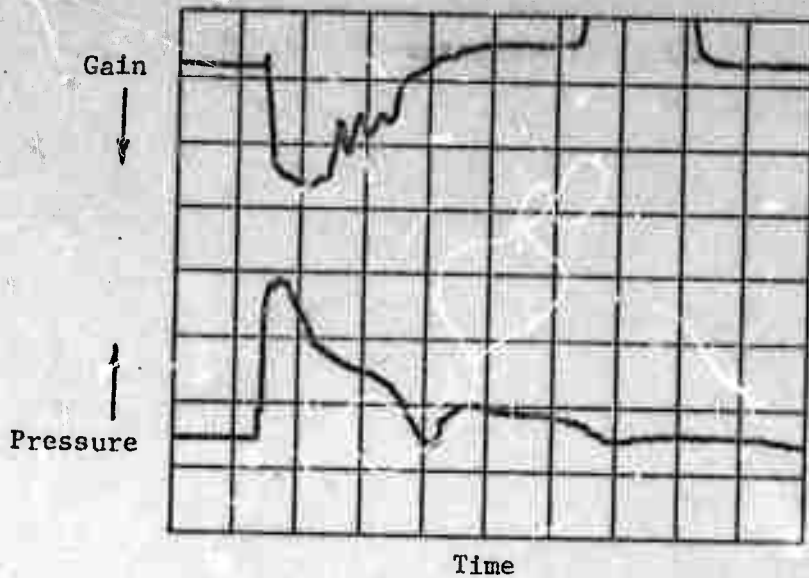
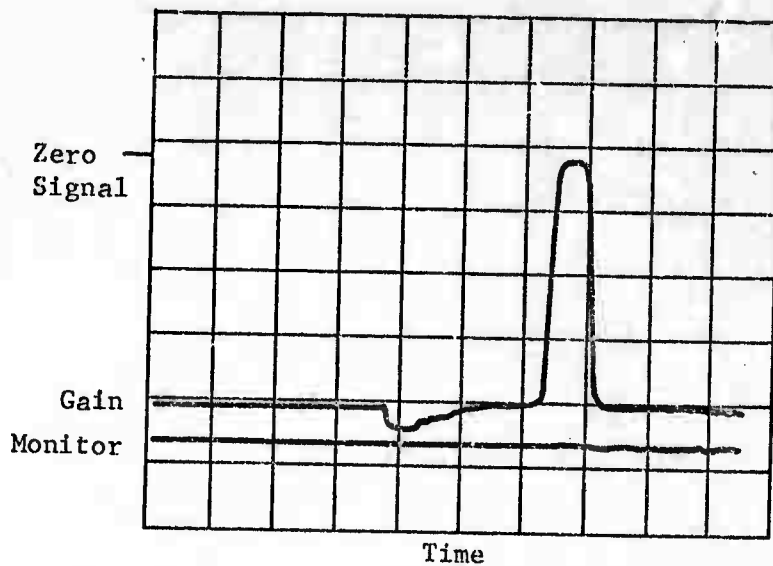


Figure 2. Sketch of the laser optical system and test section used to measure gain. (d = diffuser plate, f = 10.6 μ filter, bs = beam splitter, m = mirror, w = germanium window).



(a) Short time trace oscillograph. Vertical Scales: Gain (10mv/division), pressure (250psi/division); Horizontal Scale: Time (1msec/division).



(b) Long time trace oscillograph. Vertical scales: Gain (50mv/division), Monitor (5mv/division); Horizontal scale: Time (2 msec/division).

Figure 3. Typical oscillographs for an experimental run. Results for the 5.18% CO₂ gas mixture are shown. Measured gain = .55/meter at T₀ = 2400°K and p₀ = 39.8 atm.

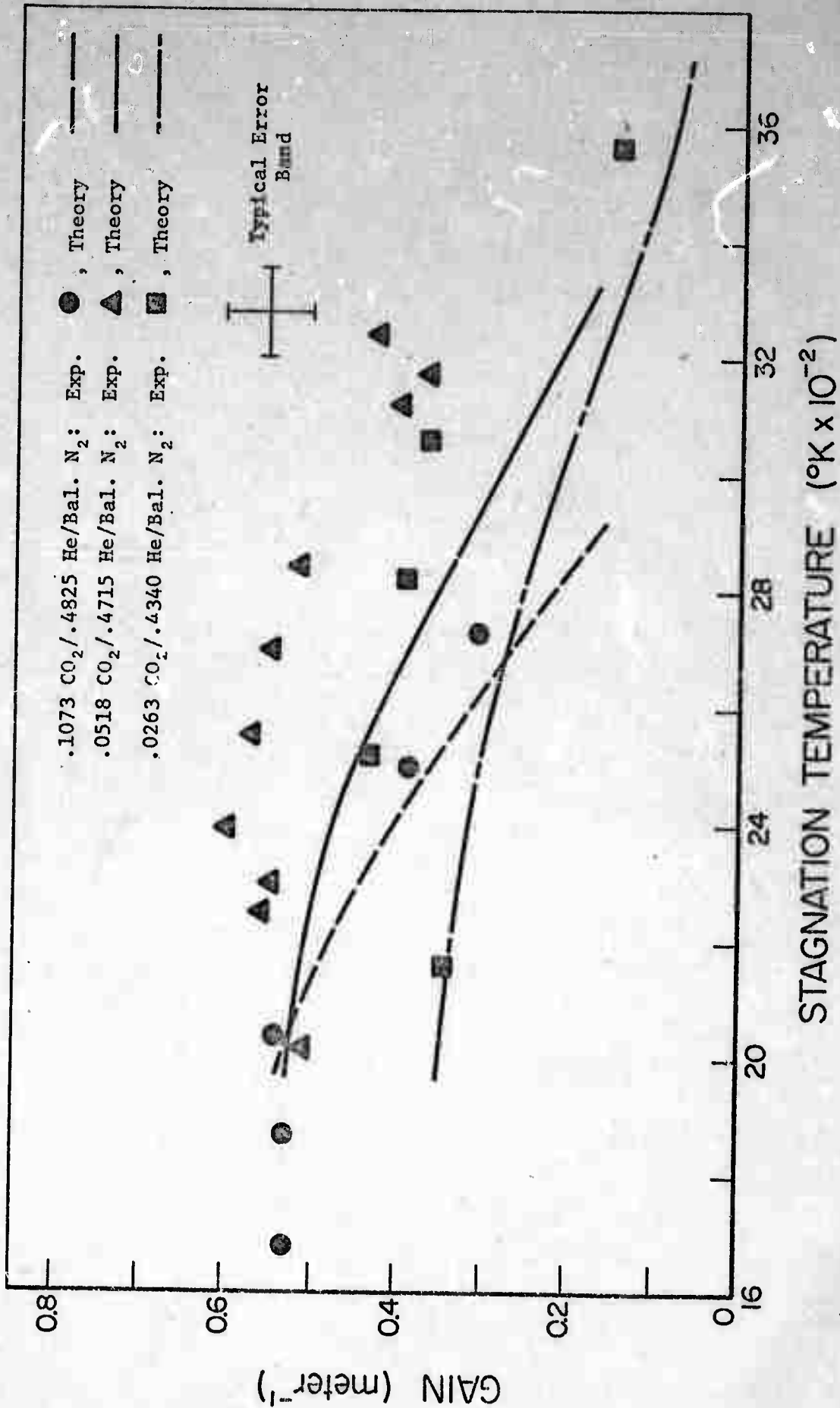


Figure 4. Gain vs. Stagnation Temperature at the Mach 5 station of a 2-D nozzle (throat height = 0.1 cm, 15° half angle). Stagnation pressure is 40 ± 5 atms. Stagnation temperatures are not corrected for dissociation effects.

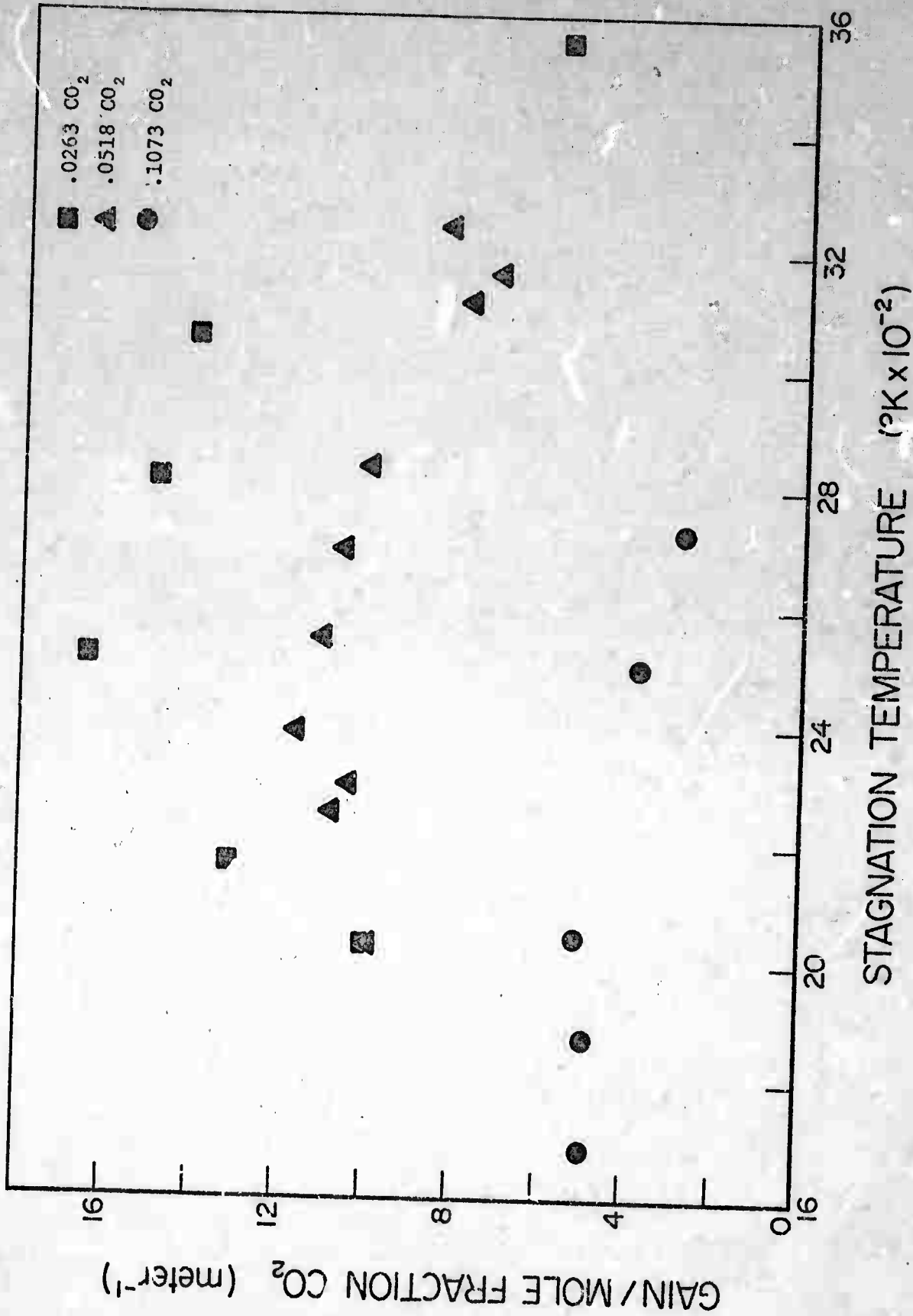


Figure 5. Gain per mole fraction of CO₂ vs. Stagnation temperature at the Mach 5 station of a 2-D nozzle. Stagnation pressure is 40 ± 5 atms.

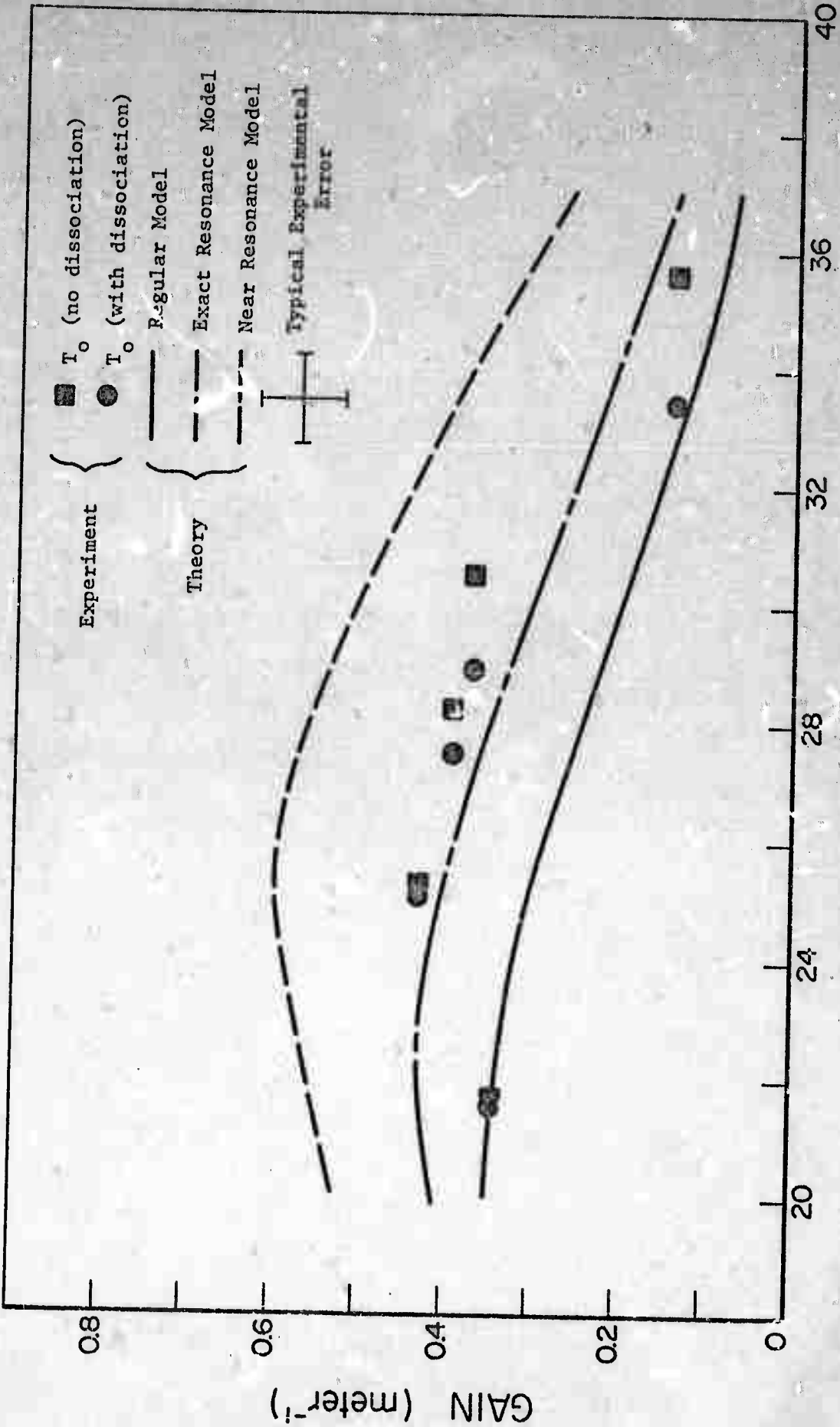


Figure 6. Gain vs. Stagnation Temperature for the 2.63% CO₂ gas mixture illustrating the predicted values for gain based upon the regular model and resonance models. The correction to the experimental data for changes in the stagnation temperature due to dissociation are also illustrated.

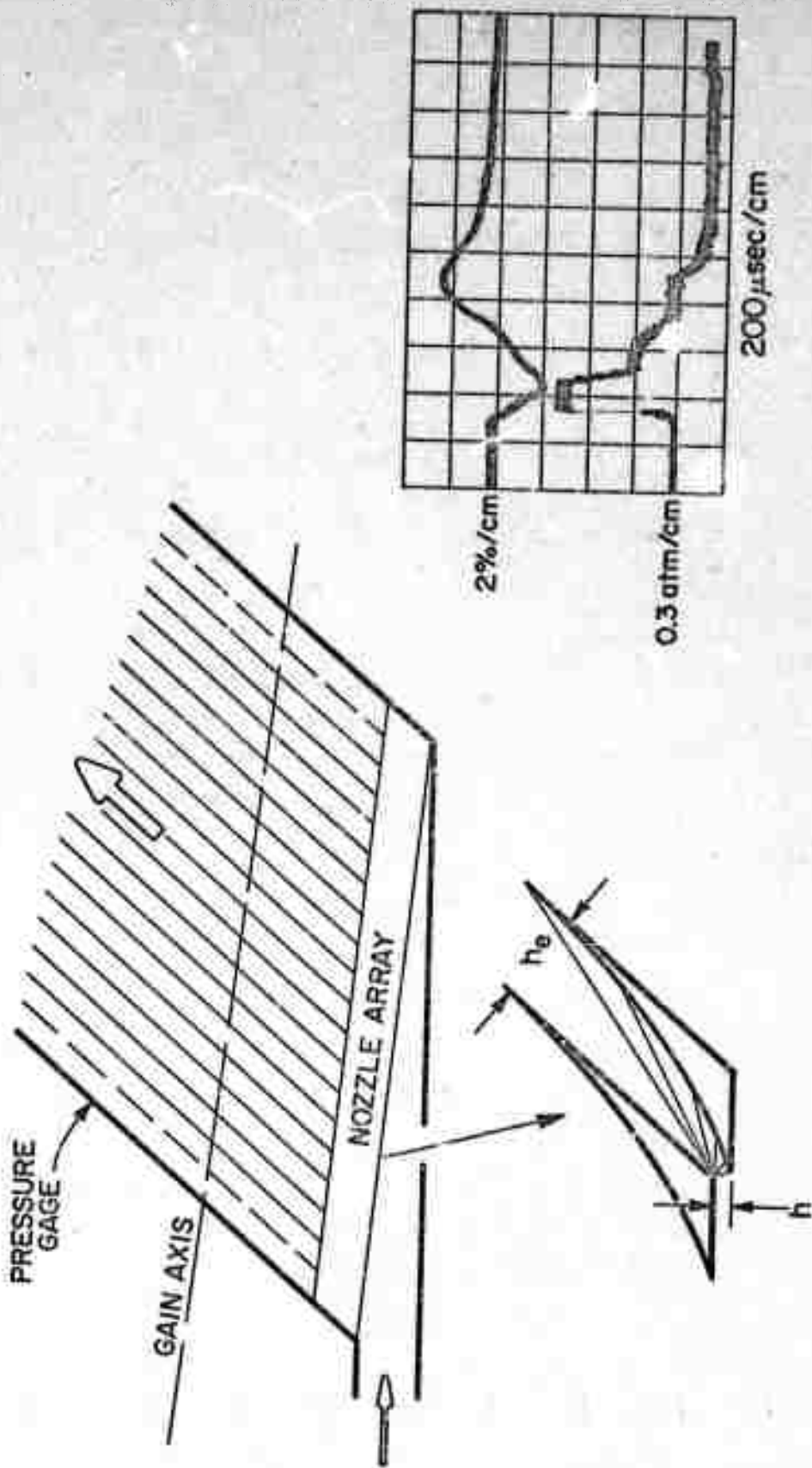


Figure 7. Turning Nozzle Geometry and Sample Gain Experiment Results.
 (see text for details)

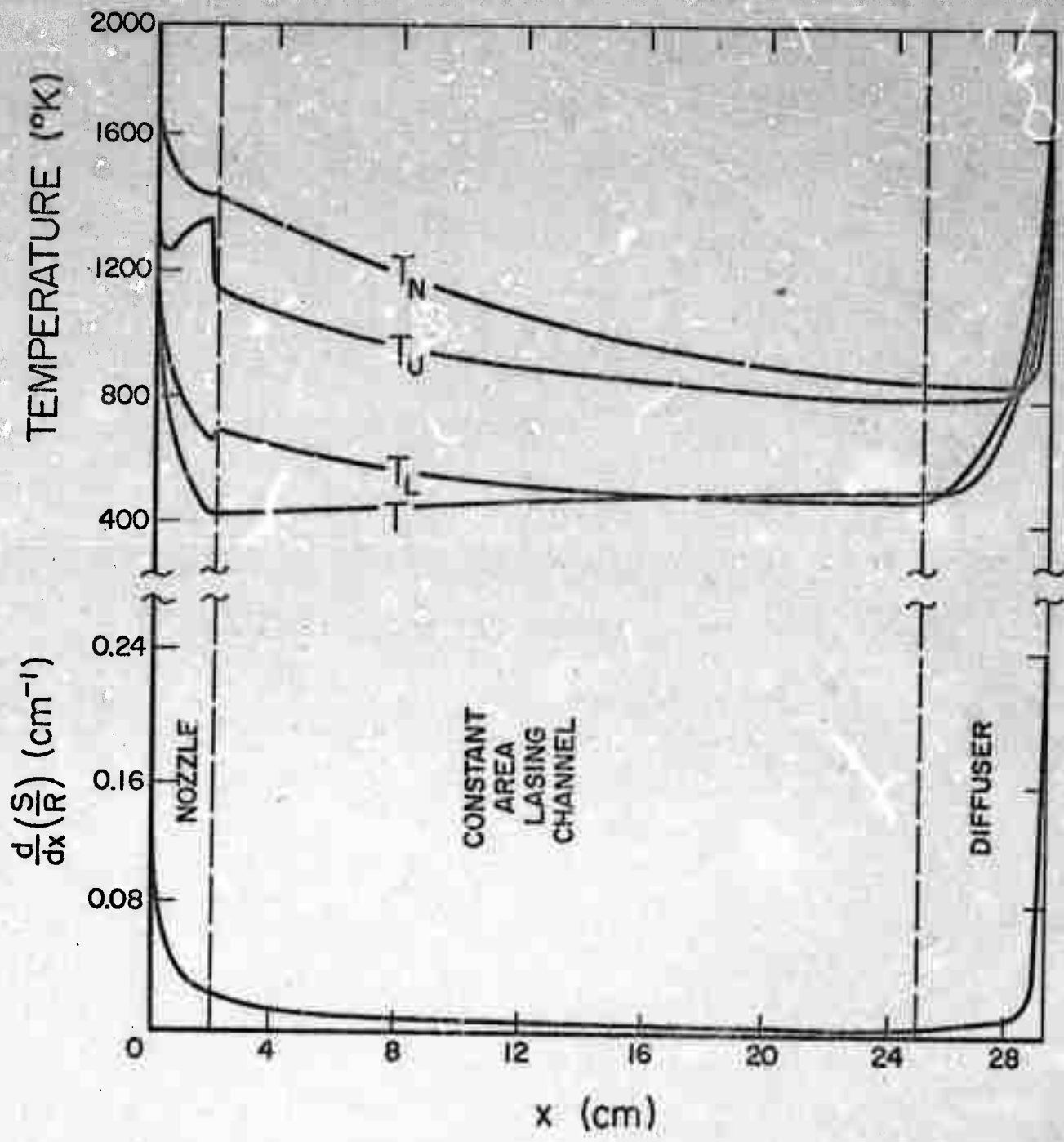


Figure 8. Temperature and Entropy Production in a Representative Supersonic Nozzle-Cavity-Diffuser Combination (see text for details)

APPENDIX A

Submitted for Publication

A Calculation of Mixed Mode Contributions
to Absorption in CO_2 at 10.6μ

S. A. Munjee and Walter H. Christiansen*

Aerospace Research Laboratory, University of Washington
Seattle, Washington 98195

A rise of temperature in a molecular system causes the higher energy levels to become more populated. For the case of CO_2 absorption (or, in a lasing medium, gain) calculations based only on single line considerations are sometimes inappropriate as the contributions from some higher energy levels can be appreciable. This note summarizes this effect for the 10.4μ band of CO_2 . The calculations are compared with the experimental measurements of others.

The equilibrium absorption contributions to the P-branch $00^0_1 \rightleftharpoons 10^0_0(\text{P}\Sigma)$ transitions due to near resonant transitions from mixed modes of the type $0X^{\ell}_1 \rightleftharpoons 1X^{\ell}_0$ have been estimated, where X is any positive integer and ℓ , the angular momentum quantum number, has appropriate values. For the range of 296°K to 800°K , it was determined that only the R-branch transitions $01^1_1 \rightleftharpoons 11^1_0(\text{R}\pi)$ and $02^0_1 \rightleftharpoons 12^0_0(\text{R}\Sigma)$ contribute significantly to the overall absorption of the P-branch lines because near resonances along with appreciable population of energy levels exist only for these transitions. For example, the $02^2_1 \rightleftharpoons 12^2_0(\text{R}\Delta)$ transitions cannot contribute because their wavelengths are not sufficiently close to those of the $\text{P}\Sigma$ lines; on the other hand, the transition of the type, $00^2_2 \rightleftharpoons 10^2_1$, may have close resonances, but the population of those states are too small.

*Assoc. Prof., Dept. of Aeronautics and Astronautics

For the calculations, vibrationally non-degenerate energy levels of molecules of a gas at moderate pressure (collision broadened) are assumed, for which the absorption coefficient at line center for a single spectral line can be written as:¹

$$\alpha(\lambda_{UL_0}) = -\frac{1}{4\pi} \frac{\lambda_{UL_0}}{\tau_{UL}} [N_U - \frac{g_U}{g_L} \frac{N_L}{\nu_C}] \quad (1)$$

where the subscripts U and L refer respectively to the upper and lower levels of the rotational-vibrational transition, λ_{UL_0} is the wavelength of the spectral line center, τ_{UL} is the radiative lifetime for the line, the g's are the rotational statistical weights, and the N's are the population densities of the rotational-vibrational quantum levels. The optical broadening collision frequency ν_C is $N\bar{a}\sigma$, here, N is the number density, \bar{a} is the mean relative speed of the molecules, and σ is the optical broadening cross section.

If a Lorentzian profile is assumed for a single spectral line of wavelength λ the absorption coefficient in the neighborhood of the line center may be expressed as:²

$$\alpha(\lambda) = \frac{\alpha(\lambda_{UL_0})}{1 + \left[\frac{2\pi c}{\nu_C} \left(\frac{1}{\lambda} - \frac{1}{\lambda_{UL_0}} \right) \right]^2} \quad (2)$$

The total absorption coefficient is then obtained by repeatedly applying Eq. (2) to contributing transitions and summing; i.e.,

$$\alpha(\lambda) = \alpha_{P\Sigma}(\lambda) + \alpha_{R\Sigma}(\lambda) + 2\alpha_{R\pi}(\lambda) \quad (3)$$

Each of the terms on the right hand side of Eq. (3) is a sum of contributions from the vibrational-rotational lines within each transition, and the coefficient 2 in its rightmost member accounts for the two-fold vibrational degeneracy of the π states. [When Eq. (1) is applied to the $R\pi$ transitions, the π

states are treated as though they were vibrationally non-degenerate, with their populations given by the Boltzmann distribution.]

In order to evaluate Eq. (3) [in terms of Eq. (1)], the radiative lifetime for spontaneous emission must be known. This is related to the Einstein coefficient for stimulated emission, and can be expressed [Eq. (2.17), Ref. 3] in terms of the J dependent and vibrational (J independent) contributions to the transition moment. Thus,

$$\frac{1}{\tau_{UL}} = \frac{64\pi^4}{3h} (\lambda_{UL_0})^3 \frac{S(J_U)K_{UL}}{g_U} \quad (4)$$

where h is Planck's constant; $S(J_U)$, the rotational contribution is taken from p. 127 and p. 208 of Ref. 4, and K_{UL} is the matrix element of the dipole moment squared. To obtain the radiative lifetime for the $P\Sigma$, $R\Sigma$, and $R\Pi$ transitions, K_{UL} is treated as a constant. Such an approximation seems reasonable because these radiative transitions do not involve a change in the quantum number of the bending mode of CO_2 . The numerical value of K_{UL} (1.37×10^{-39} erg-cm³) is obtained by applying Eq. (4) to the P(20) line of the $P\Sigma$ transition with $\tau_{UL} = 5.38$ sec.⁵ Different authors^{6,7} have reported a weak variation in line width (hence σ) with the rotational quantum number for the $P\Sigma$ transition. However, variations between authors show wider differences than the variation with rotational quantum number. Furthermore, this dependence for transitions other than the $P\Sigma$ has not been established. In the calculations therefore, σ has been considered a constant with its value (1.3×10^{-14} cm²) taken from Ref. 8.

Finally, the various wavelengths (λ_{UL_0}) needed to complete the evaluation of Eq. (3) can be obtained from Eqs. (5.1) - (5.4) once the rotational-vibrational constants of the molecule are known.⁹

$$P\Sigma: (\lambda_{UL_0})^{-1} = E_0 + B_U[J(J-1)] - B_L[J(J+1)] \quad (5.1)$$

$$P\pi: (\lambda_{UL_0})^{-1} = E_0 + B_U[J(J-1) - \ell^2] \quad (5.2)$$

$$- B_L[J(J+1) - \ell^2] + \frac{(-1)^J}{2} [q_U J(J-1) - q_L J(J+1)]$$

$$R\Sigma: (\lambda_{UL_0})^{-1} = E_0 + B_U[(J+1)(J+2)] - B_L[J(J+1)] \quad (5.3)$$

$$P\pi: (\lambda_{UL_0})^{-1} = E_0 + B_U[(J+1)(J+2) - \ell^2] - B_L[J(J+1) - \ell^2] \\ + \frac{(-1)^J}{2} [q_U (J+1)(J+2) - q_L J(J+1)] \quad (5.4)$$

In Eqs. (5.1) - (5.4), E_0 is the difference between the vibrational energy (E_{vib}) of the upper and lower levels, expressed in cm^{-1} . The B's are the rotational constants, and the q's are the ℓ -type doubling constants, both of which are expressed in cm^{-1} ; J is the rotational quantum number of the lower level. The calculation of the B's and q's cannot be readily accomplished because the lower levels of each of the 3 transitions are in Fermi Resonance with other levels of the molecule. For the P Σ transition, the constants were taken from Ref. 10, for the R Σ transition from Ref. 11, and for the R π transition from Ref. 12. This is summarized in Table I. Using the values in Table I and Eqs. (5.1), (5.3) and (5.4), "near resonances" were calculated; these are shown in Table II for some selected J_L values of the P Σ transition.

Calculations of the total absorption coefficient [Eq. (3)] for the wavelengths of the P Σ transitions were carried out for values of J_L from 14 through 28. Because of interest in the strong P(20) laser line, results for this wavelength are shown in Fig. 1. This figure compares the results of calculations made in this study with the experimental measurements of Refs. 14 and 15. The broken curve represents α_0 , the single line center absorption coefficient for the P(20) line only. The solid curves represent α , the total absorption coefficient, which is comprised of α_0 and contributions from mixed modes. Interest has persisted in the R π (23) line and the P Σ (20) line as these two are believed to be very nearly resonant. The authors of

Ref. 14 believe this difference to be within several hundredths of a wave-number; in this study (Table II) the difference is estimated as $.011 \text{ cm}^{-1}$.

In the lower temperature range ($296^\circ\text{K} - 425^\circ\text{K}$) the calculation of α for $p = 1/3 \text{ atm}$. is compared with the experimental measurements of Ely & McCubbin.¹⁴ While there is considerable scatter in the data Figure 1 indicates that the calculated values of α are generally somewhat lower than those measured. However, if the uncertainty of $\pm 8\%$ indicated in Ref. 14 is assumed to apply throughout the lower temperature range, the agreement is better. The contributions from the mixed modes at 300°K is seen to be about 6.4% . Ref. 14 estimates it as 3.2% based on the assumption that the line intensity ratios depend only upon the Boltzmann factors and the $(2J+1)$ degeneracies. If allowance is made for the two-fold vibrational degeneracy of the π states, the estimate of 3.2% will be doubled. Also, Eq. (2) of Ref. 14 does not seem to allow for the temperature dependence of the rotational populations.

In the higher temperature range (above 400°) the calculations of α ($p = 1 \text{ atm}$) are compared with the measurements of Leonard.¹⁵ Although Leonard's data exhibit a fair amount of scatter the figure indicates that the total absorption (α) is considerably greater than the single line center absorption (α_0). At 400°K , for instance, the calculated contribution is about 17.7% and at 620°K it is 42.1% . The figure also suggests that the measurements correspond more closely to α than to α_0 . Calculations of α for $\text{P}\Sigma(14)$, $\text{P}\Sigma(16)$ and $\text{P}\Sigma(18)$ have been compared with Leonard's data¹⁵ and it was concluded that the calculations agreed with his data to within 10% . Without the mixed mode contribution, the difference was as much as four times that.

Figure 2 shows the quantity $\Omega = (\alpha/\alpha_0 - 1)$ as a function of pressure (for some selected temperatures) for the case of $\text{P}\Sigma(20)$. The results for other lines are similar in trend; Ω tends to increase with pressure, then

levels off, and increases once again. For very close resonances such as the $P\Sigma(28) - R\Pi(12)$, $(\frac{\partial\Omega}{\partial p})_T \approx 0$ for pressures approximately .05 atm to 1 atm. This characteristic is shown in Figure 2 as the two broken curves (for $T = 296^\circ\text{K}$ and $T = 800^\circ\text{K}$). For wavelength differences greater than $5\%B$ ($B \approx .39 \text{ cm}^{-1}$) there is no extended region of pressure for which this characteristic is observed.

The absolute magnitude of the mixed mode contributions are questionable primarily because the rotational-vibrational constants of the molecule are not known with adequate precision. Despite this, the behavior of Ω can be expected to be similar to that in Figure 2. This is so because for a given value of "near resonance" [$\Delta = \frac{1}{\lambda} - \frac{1}{\lambda_{UL_0}}$ in Eq. (2)] the effect of the uncertainty in Δ can be offset by a compensating change in ν_C , i.e., a different pressure. This suggests that a sensitive experiment conducted to identify $(\frac{\partial\Omega}{\partial p})_T$ would enable better values of the rotational-vibrational constants to be inferred.

In review, it is believed that the inclusion of the contributions of the mixed modes gives satisfactory agreement with experiments on absorption at 10.6μ , notwithstanding the assumptions regarding σ and K_{UL} .

The authors are grateful to Dr. G. A. Tsongas for his very helpful comments and suggestions. This work was supported by the U.S. Army Research Office (Durham).

REFERENCES

1. E. T. Gerry and D. A. Leonard, Appl. Phys. Letters, 8, 227 (1966);
Eq. (1) of Ref. 1 has been updated and modified by a factor of 2 via private communication (1970).
2. A. C. G. Mitchell and M. W. Zemansky, "Resonance Radiations and Excited Atoms" (Cambridge at the University Press, 1971) p. 160.
3. J. C. Polyani, App. Opt. Suppl. (Chemical Lasers) 2, 109 (1965).
4. G. Herzberg, "Molecular Spectra and Molecular Structure I; Spectra of Diatomic Molecules" (Van Nostrand Reinhold Co., 1950).
5. Private communication with E. T. Gerry (1971).
6. C. Rosetti, R. Farrenq and P. Barchewitz, J. Chem. Phys. 64, 93 (1967).
7. U. P. Oppenheim & A. D. Devir, J. Opt. Soc. Am. 58, 585 (1968).
8. C. Freed and A. Javan, Appl. Phys. Letters, 17, 53 (1970).
9. The shift in wavelength due to a change in pressure has been neglected because the data in Ref. 8 suggests that it is small with respect to the line width.
10. C. K. N. Patel, Phys. Rev. 136, A1187 (1964).
11. R. H. Tourin and P. M. Henry, "Infrared Spectral Emissivities and Energy Distribution of CO₂ at High Temperatures." Part I: Internal Energy Calculations. (The Warner & Swasey Co., Control Instrument Div., 34 W 33 St., N. Y., Dec. 1958).
12. J. A. Howe and R. A. McFarlane, J. Mol. Spectry. 19, 224 (1966). It is possible to calculate some of the constants. From Eq. (11) Ref. 16 $B_{01^1_1} = .387896 \text{ cm}^{-1}$. Using Eq. (14) of Ref. 16 and appropriate values from pp. 274, 211, and 276 of Ref. 13, $B_{11^1_0} = .2908131 \text{ cm}^{-1}$. Also Ref. 16 gives $q_{01^1_1} = 6.15 \times 10^{-4} \text{ cm}^{-1}$. However, $q_{11^1_0}$ is not readily calculable.

Using the values in Table I and Eq. (5.2), the entries in Table I of Ref.12 are very nearly reproduced.

13. G. Herzberg, "Molecular Spectra and Molecular Structure II, Infrared and Raman Spectra of Polyatomic Molecules" (D. Van Nostrand Co. Inc., N. J., 1968).
14. R. Ely and T. K. McCubbin Jr., Appl. Opt. 9, 1230 (1970).
15. R. L. Leonard, Thesis Ph.D., University of Washington, Seattle, WA (1972).
16. C. P. Courtoy, Can. J. Phys. 35, 608 (1957).

TABLE I
SUMMARY OF ROTATIONAL VIBRATIONAL CONSTANTS

(All values in the body of the table are in cm^{-1})

	PΣ		RΣ		RT	
	00 ¹	10 ⁰	02 ¹	12 ⁰	01 ¹	11 ⁰
E ₀		960.94		939.85		927.17*
E _{vib}	2349.24	1388.3**	3612.85***	2673.00***	3003.67	2076.5**
B	.3866	.3897	.38783	.39017	.3879	.39093
q	-	-	-	-	.00062	.00091

* Average of 'c' and 'd' levels in Ref. 12

** Table 56, p. 274, Ref. 13

*** Table V, p. 15, Ref. 11

TABLE II
NEAR RESONANCES

(Wavelengths Expressed in cm^{-1})

P Σ		R Σ			R Π		
J _L	Eq. (5.1)	J _L	Eq. (5.3)	Eq. (5.1) - Eq. (5.3)	J _L	Eq. (5.4)	Eq. (5.1) - Eq. (5.4)
14	949.464	12	949.569	-.104	32	949.442	.022
18	945.962	8	946.662	-.700	26	945.908	.055
20	944.174	4	943.682	.493	23	944.185	-.011
28	936.773	4*	936.698	.075	12	936.771	.002

* P-branch of the 02°1 \neq 12°0

CAPTIONS AND NOTES FOR FIGURES

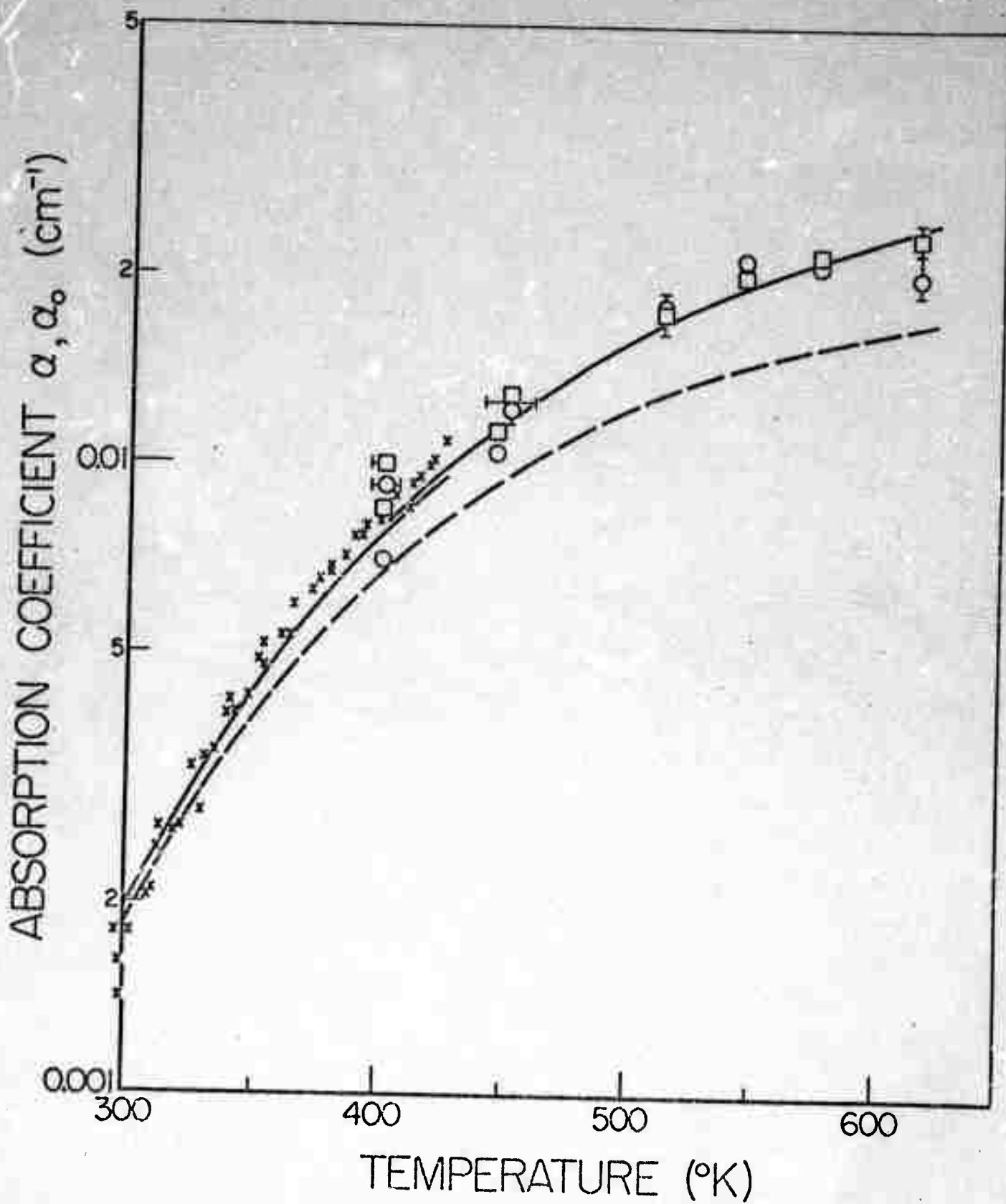
Figure 1: TOTAL ABSORPTION AND SINGLE LINE CENTER ABSORPTION FOR $P\Sigma(20)$

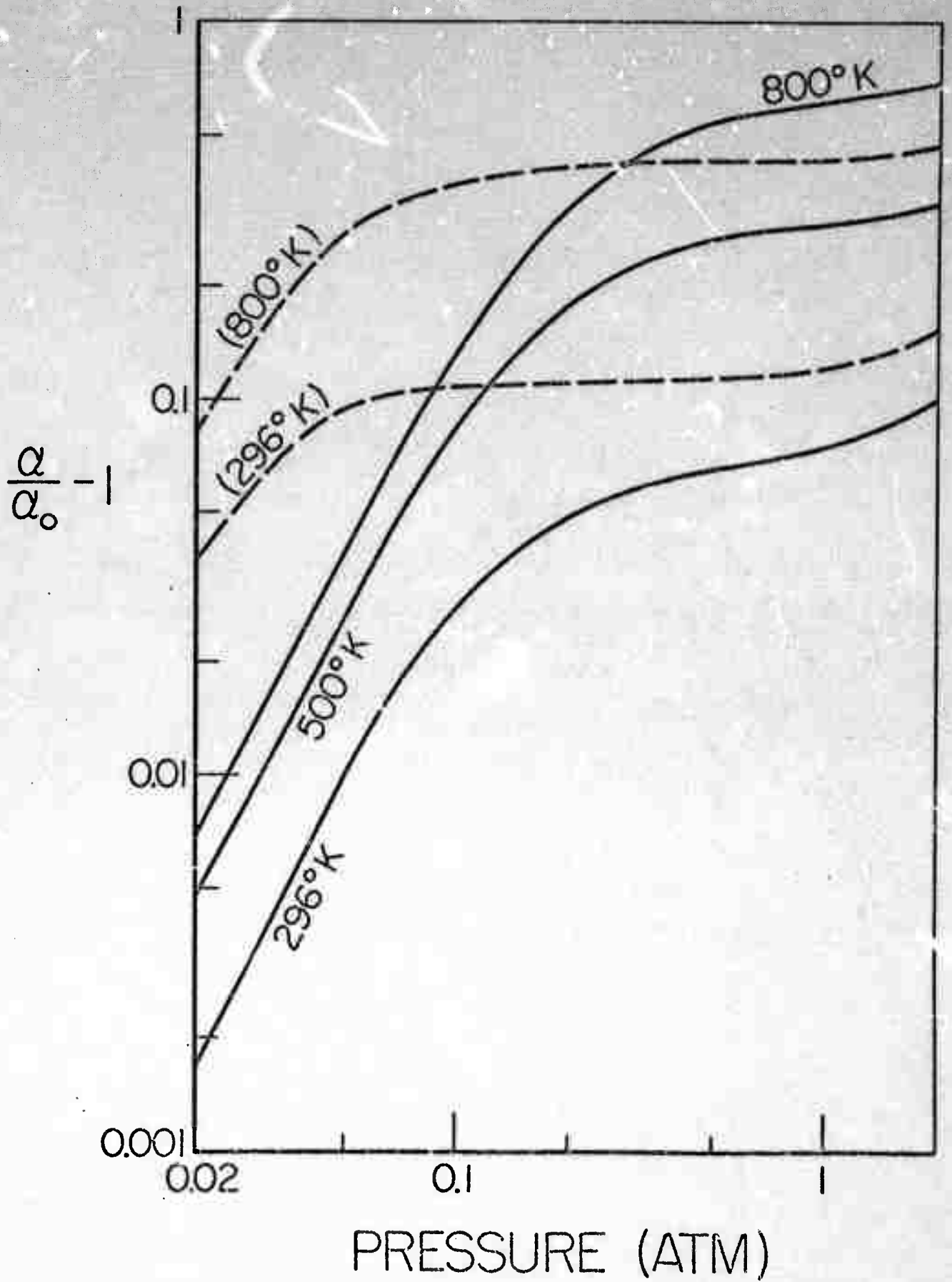
X $1/3$ atm., Ref. 14.; θ 1 atm., \square $1/2$ atm., from Ref. 15.

The broken curve is α_0 . The two solid curves are calculations of α ; the lower temperature range ($296^\circ\text{K} - 425^\circ\text{K}$) is a calculation for $p = 1/3$ atm., the higher temperature range is for $p = 1$ atm.

Figure 2: CONTRIBUTION FROM OTHER LINES TO SINGLE LINE CENTER ABSORPTION

The solid curves are for $P\Sigma(20)$ with $\alpha_0 = 1.726 \times 10^{-3} \text{ cm}^{-1} (296^\circ\text{K})$, $1.243 \times 10^{-2} \text{ cm}^{-1} (500^\circ\text{K})$, $1.766 \times 10^{-2} \text{ cm}^{-1} (800^\circ\text{K})$. The broken ones are for $P\Sigma(28)$ with $\alpha_0 = 1.14 \times 10^{-3} \text{ cm}^{-1} (296^\circ\text{K})$ and $1.858 \times 10^{-2} \text{ cm}^{-1} (800^\circ\text{K})$.





COMPUTATION OF POPULATION INVERSION IN CO₂-N₂ LASER

MIXTURES USING A FINITE NUMBER OF LEVELS

Oktay Yesil

INTRODUCTION

The invention of the laser is perhaps one of the most important technical developments of the last decade. This device has given scientists and engineers a new tool for generating coherent radiation. Their present use in many areas and their future applications have been well recorded.^{1,2}

There has been much theoretical work done on the kinetic processes of relaxational phenomena. In some of their previous works, Rubin and Shuler^{3,4,5}, and Montroll and Shuler⁶ have made a theoretical study of the collisional and radiative relaxation of a system of harmonic oscillators with an infinite number of levels. Using the Boltzmann's formula and under the assumption that the quantum energy is very much less than kinetic energy (i.e., $h\nu/kT \ll 1$), they obtained the vibrational relaxation master equations. They found that the detailed relaxation behavior depends strongly on the form of the collisional probabilities and that radiative transitions do not change the relaxation behavior of the system.

Basov et al⁷, on the other hand, have carried out the kinetics of systems by mode analysis rather than on an individual level basis. Using mode analysis, many authors have analyzed the population inversions of CO₂-N₂ laser mixtures in rapid expansion nozzles using the generalized energy-level diagram (fig. 1) and have calculated the gain between the levels (00¹)-(10⁰) of CO₂, $\lambda = 10.6$ micron.

To the best of our knowledge, the possibility of obtaining gain between the levels (02⁰)-(01¹0) of CO₂, 16.8 μ (simultaneously when lasing the CO₂ molecule at 10.6 μ) has not been reported so far. Hence, this work is undertaken.

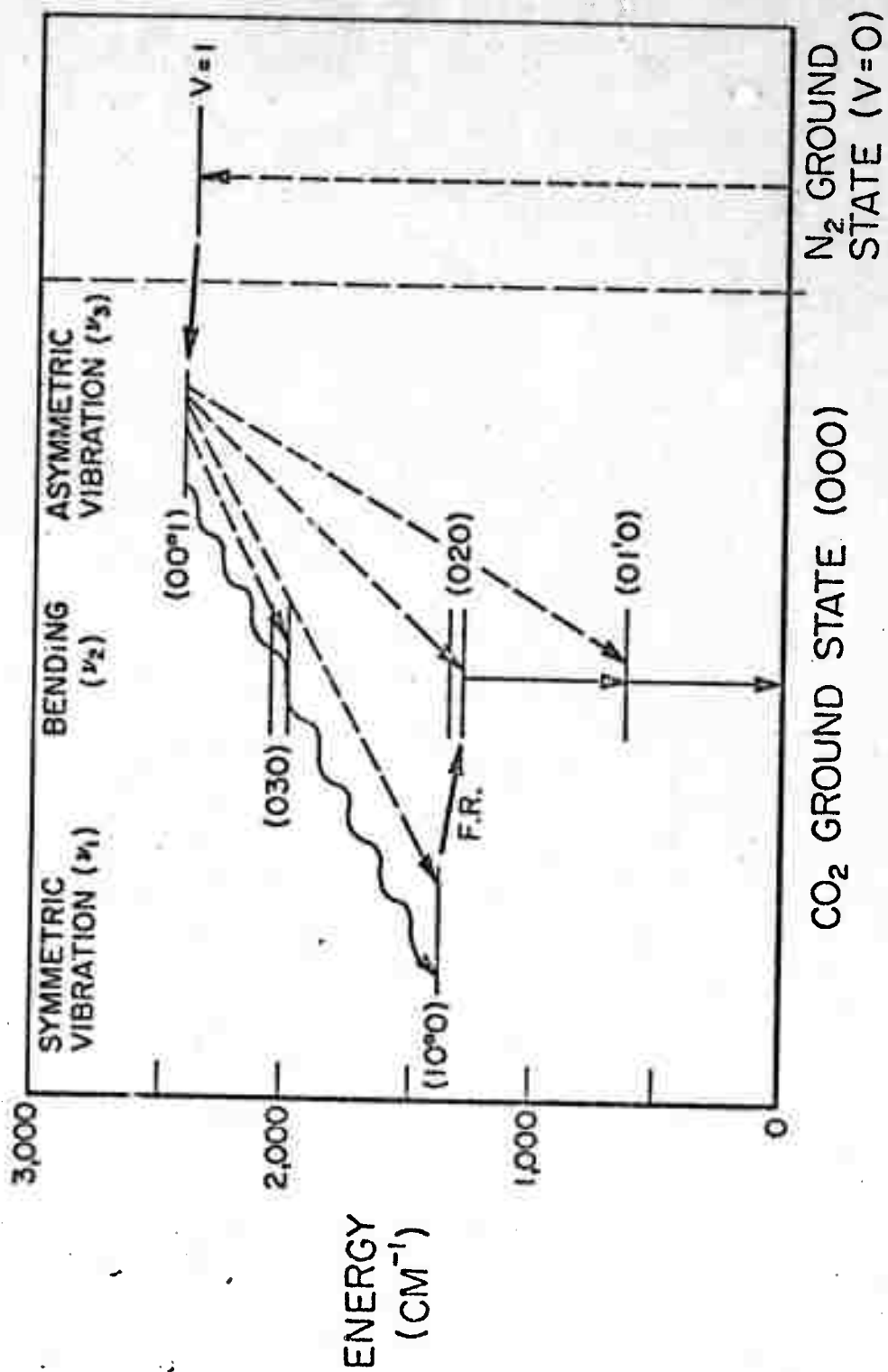


FIGURE 1. GENERALIZED PARTIAL ENERGY DIAGRAM OF CO₂-N₂ MIXTURE

This work is devoted to the establishment of the conditions under which sufficient gain between the levels $\text{CO}_2(00^01)-\text{CO}_2(10^00)$, 10.6μ , as well as between $\text{CO}_2(02^00)-\text{CO}_2(01^10)$, 16.18μ , is obtained in CO_2-N_2 -He laser gas mixtures, varying gas concentrations and the ratios of vibrational to translational temperatures. Initial number densities of all vibrational levels were taken as zero except $\text{CO}_2(00^01)$ and $\text{N}_2(v=1)$, which were given a Maxwell-Boltzmann temperature of 3000°K . The gas was held at a constant pressure of 1 atmosphere (14.7 psi). Because of the complexity, a finite number of levels of harmonic oscillators has been considered, and the vibration to vibration (V-V) transitions have been neglected. Actually, since V-V transitions are faster than the others, we have investigated the effects of their absence. Practically, this can be achieved by reducing CO_2 -concentrations. Therefore, we dealt with low CO_2 -concentrations only (up to 10% by molar fraction) in the calculations.

THE CO_2-N_2 SYSTEM

CO_2 is a linear triatomic molecule. It has four vibrational degrees of freedom: the symmetric stretch mode ν_1 , the doubly-degenerate bending mode ν_2 , and the asymmetric stretch mode ν_3 . N_2 is a symmetric diatomic molecule. It has only one vibrational degree of freedom which is commonly designated by v . (see figure 1).

We have considered a CO_2-N_2 system for which the kinetics are well known^{8,9} and which was initially excited to a nonequilibrium vibrational distribution by different methods^{4,7,8}. In our work, the levels of the system have been allowed to reach a quasi-steady-state condition; then strong lasing at 10.6μ has been turned on by Q-switching a laser cavity. This quickly bleaches the $\text{CO}_2(00^01)$ to $\text{CO}_2(10^00)$ transition, which increases the

CO₂(02°0) population, through Fermi-resonance, to give a population inversion between CO₂(02°0) and CO₂(01°0) levels. Here we have used the level analysis rather than the mode analysis. It cannot be used since we hope to get an inversion within a mode (i.e., negative temperature) during lasing, and therefore the mode is not in equilibrium as the mode analysis assumes.

MODEL

Figure 2 shows the newly developed schematic model of the major participating vibrational energy levels for CO₂-N₂ laser gas mixtures. This was done by writing down all the possible levels in the order of increasing value of their vibrational energies until the cut-off line (strong dashed line at E=3775 cm⁻¹). Energy is measured from the ground state of CO₂(00°0) and N₂(v=0) and only the pertinent vibrational levels (totalling 25) have been shown. The effect of levels above the cut-off line has been neglected because the higher levels have many fewer particles at this vibrational temperature.

The population of levels becomes redistributed as the temperature changes according to the Boltzmann's formula:

$$\frac{n_{i+1}}{n_i} = \exp\left[-\frac{\Delta E}{kT_v}\right] \quad (1)$$

where ΔE is the energy difference between the levels $i+1$ and i of a single mode.

Each of the vibrational levels shown is split into a series of sublevels due to the quantized rotational energies of the molecules as a whole, but these are not indicated. Table I shows the vibrational energy levels of CO₂-N₂ mixture. Column 1 gives the levels and Column 2 shows the

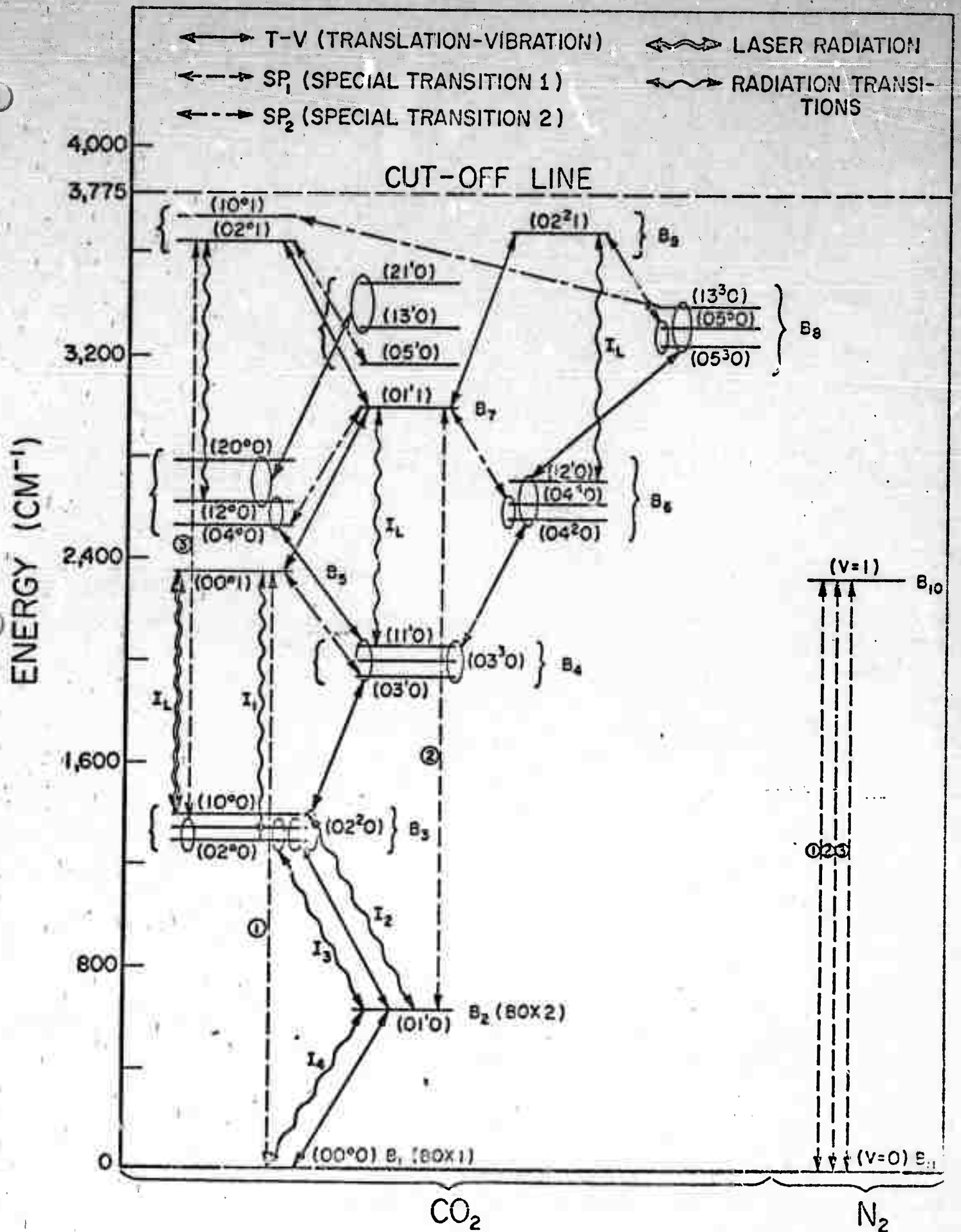


FIGURE 2. SCHEMATIC MODEL FOR A (CO₂-N₂) SYSTEM

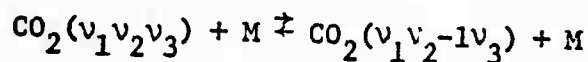
LEVEL	ENERGY	DEGENERACY
$v_1 \quad v_2 \quad v_3$	-1 cm	g_l
0 0 ⁰ 0	0.00	1
0 1 ¹ 0	667.30	2
0 2 ⁰ 0	1285.38	1
0 2 ² 0	1335.11	2
1 0 ⁰ 0	1388.13	1
0 3 ¹ 0	1932.45	2
0 3 ³ 0	2003.88	2
1 1 ¹ 0	2076.86	2
0 0 ⁰ 1	2349.14	1
0 4 ⁰ 0	2551.10	1
0 4 ² 0	2583.60	2
0 4 ⁴ 0	2672.80	2
1 2 ⁰ 0	2673.00	1
1 2 ² 0	2760.63	2
2 0 ⁰ 0	2797.05	1
0 1 ¹ 1	3003.94	2
0 5 ¹ 0	3183.80	2
0 5 ³ 0	3241.30	2
1 3 ¹ 0	3338.90	2
0 5 ⁵ 0	3341.80	2
1 3 ³ 0	3442.30	2
2 1 ¹ 0	3500.50	2
0 2 ⁰ 1	3612.85	1
0 2 ² 1	3659.30	2
1 0 ⁰ 1	3714.59	1
N(v=C)	0.00	1
N(v=1)	2367.14	1

corresponding energies in cm^{-1} . Column 3 gives the multiplicity (or degree of degeneracy) of the levels. This multiplicity occurs only for v_2^{10} .

In the model, { } 's in fig. 2 contain the levels which have nearly equal energies and each { } has been labeled as B_1 (Box₁), B_2 , B_3 , etc. Hence, fast transitions appear to justify a vibrational model which groups the participating levels into 11 boxes. It is assumed there is local equilibrium within each box but not between boxes.

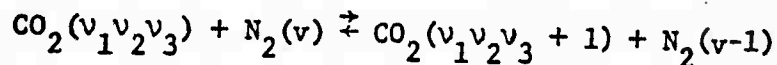
In this work, only the following relaxation processes have been considered¹¹:

1. Translation to vibration (T-V), strong solid lines

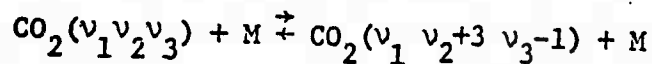


2. Special transitions (SP)

- a) SP_1 , light dashed lines



- b) SP_2 , light long dashed lines.



3. Radiation transitions (RAD), wavy lines

Here, M is called the collision partner and $M = \text{CO}_2, N_2$ or He.

We note that (V-V) transitions have been neglected. Because the probability of them, $P_{V-V} \sim 10^{-3}$ ⁽¹²⁾ i.e., they are about 10 times faster compared to the other transitions in our work.

GOVERNING EQUATIONS

1. Master vibrational relaxation equations

Formally, any simple, linear relaxation process can be described by an equation:

$$\frac{dU}{dt} = -\frac{1}{\tau} (U - U_e)$$

where U is quantity which is relaxing and U_e is its equilibrium value.
 τ is the characteristic time of the relaxation process.

The master vibrational relaxation equation for the number density, n_i at level i , contains the terms of all possible relaxation processes, i.e.,

$$\left. \frac{dn_i}{dt} \right|_T = \left. \frac{dn_i}{dt} \right|_{T-V} + \left. \frac{dn_i}{dt} \right|_{V-V} + \left. \frac{dn_i}{dt} \right|_{V-V} + \left. \frac{dn_i}{dt} \right|_{RAD}$$

(intra mode) (inter mode)

Neglecting (V-V) transitions and including the special transitions, and introducing the fraction of the level i , x_i ($\equiv \frac{n_i}{N}$, N is the total number of particles) we have:

$$\left. \frac{dx_i(t)}{dt} \right|_T = \left. \frac{dx_i}{dt} \right|_{T-V} + \left. \frac{dx_i}{dt} \right|_{SP} + \left. \frac{dx_i}{dt} \right|_{RAD}$$

For the complete set of master vibrational relaxation equations used in the computer program see the Addendum.

2. Equations for the Gain Calculations

From reference (13), the expression of the line center gain coefficient for a collisionbroadened line, is given by

$$\alpha = \frac{\lambda^2}{4\pi\tau(\pi\Delta\nu_c)} g_J \left(\frac{n_J}{g_J} - \frac{n_{J'}}{g_{J'}} \right) \quad (2)$$

where $\Delta\nu_c$ is the line width and is related to the collisional frequency, ν_c by $\nu_c = \pi\Delta\nu_c$.

The expression for ν_c , in the case CO_2-N_2-He mixture, is:

$$v_c = N_{CO_2} [\sigma_{CO_2} \bar{c}_{CO_2} + \frac{N_{He}}{N_{CO_2}} \sigma_{He} \bar{c}_{He} + \frac{N_{N_2}}{N_{CO_2}} \sigma_{N_2} \bar{c}_{N_2}] \quad (3)$$

where N's are the population density of the species, σ 's are the collision cross-section of each species with CO_2 ,

$$\sigma_{CO_2} = 1.3 \times 10^{-14} \text{ cm}^2$$

$$\sigma_{He} = 3.7 \times 10^{-15} \text{ cm}^2$$

$$\sigma_{N_2} = 8.7 \times 10^{-15} \text{ cm}^2$$

\bar{c} 's are the mean relative velocity of the species, $\bar{c}_i = \sqrt{\frac{8kT}{\pi\mu_i}}$, $\frac{1}{\mu_i} = \frac{1}{m_{CO_2}} + \frac{1}{m_i}$.

λ is the transition wavelength, and

$$\lambda = \begin{cases} 10.6\mu & \text{for the radiation between } CO_2(00^{\circ}1) - CO_2(10^{\circ}0) \\ 16.18\mu & \text{for the radiation between } CO_2(02^{\circ}0) - CO_2(01^{\circ}0) \end{cases}$$

τ is the radiative life time for the transition, and from reference (14)

$$\tau = \begin{cases} 4.17 \text{ sec.} & \text{for the radiation at } 10.6\mu \\ 2.08 \text{ sec.} & \text{for the radiation at } 16.18\mu \end{cases}$$

n_J is the number of particles in the Jth rotational band of the upper level.

$n_{J'}$ is the number of particles in the J'th rotational band of the lower level.

g_J is the rotational degeneracy, and $g_J = 2J + 1$

$$g_{J'} = 2J' + 1$$

We note that for the radiation at 10.6μ , P-branch transitions and, for the radiation at 16.18μ , Q-branch transitions give the most gain.^{10,13,14}

Furthermore, $\frac{n_J}{g_J}$ and $\frac{n_{J'}}{g_{J'}}$ in equation (2) have been evaluated in the following way for the case at 16.18μ :

$$\frac{n_J}{g_J} = \frac{n_J}{g_J n(02^{\circ}0)} \cdot \frac{n(02^{\circ}0)}{N} \cdot N \quad (\text{upper level})$$

$$\frac{n_{J'}}{g_{J'}} = \frac{n_{J'}}{g_{J'} n(01^{\circ}0)} \cdot \frac{n(01^{\circ}0)}{N} \cdot N \quad (\text{lower level})$$
(4)

On the other hand, from ref. (12),

$$\frac{n_J}{g_J n(02^{\circ}0)} \doteq \frac{1}{Q_R} \exp[-J(J+1) \frac{\theta_r}{T}]$$

$$\frac{n_{J'}}{g_{J'} n(01^{\circ}0)} \doteq \frac{1}{Q_R} \exp[-J'(J'+1) \frac{\theta_r}{T}]$$
(5)

where $Q_R \doteq \frac{T}{2\theta_r}$: rotational partition function

$\theta_r = \frac{hcB}{T} \doteq 0.56$: rotational characteristic temperature

$B \doteq 0.39$: a coefficient dependent on the vibrational level

$J = J_{\text{Max}} = \sqrt{\frac{kT}{2hcB}}$ corresponds to the peak gain

We note that, $\frac{n(02^{\circ}0)}{N}$ and $\frac{n(01^{\circ}0)}{N}$ come directly from our computer program.

For more detail, see references (10, 13, and 14).

RESULTS AND DISCUSSION

To obtain a solution for a given set of initial conditions, the coupled equations must be numerically integrated. In the set of master vibrational relaxation equations (Appendix A), the independent variable is time, t (or in nondimensional form, $t' = t \sum_{f \rightarrow 0}^M M$, see the Addendum). There are several dependent variables: the rate constants (see Appendix A) which have been obtained from experimental results given in reference (16) at the corresponding translational temperature, and the total number of particles, which has been calculated with the state equation (i.e., $P = NkT$), for the corresponding

translational temperature, T . Then the populations (or the population fractions) of the levels are computed versus time. The 10.6μ small signal gain coefficients have been calculated at $t' = 5$ (time to reach a quasi-steady-state condition), and the 16.18μ gain coefficients at $t' = 5.02$ (just after the lasing). The effect of the absorption from the level $\text{CO}_2(00^00)$ to $\text{CO}_2(01^10)$ on the gain has been analyzed and found to be unimportant for the $\text{CO}_2(02^00)$ to $\text{CO}_2(01^10)$ transition at 16.18μ .

The system of equations has been solved in FORTRAN IV, on the CDC 6400 computer (at the University of Washington) using a 5th order Runge-Kutta technique, subroutine RKINIT*¹.

This technique uses error estimates based on the comparison of two 4th order solutions; 5th order results are obtained by an extrapolation process.

Some typical results have been shown in figures 3 through 8, and tables II and III for the following data:

$P = 1 \text{ atm}$: total pressure
 $T_v = 3000^\circ\text{K}$: initial vibrational temperature
 $K_{LL} I_L = 100 \times k_f \times N$: for the laser radiation only between $\text{CO}_2(00^01)$ and $\text{CO}_2(10^00)$
 with variable T_v/T , $X_{\text{CO}_2}/X_{\text{N}_2}$ and mixture.

we note that, the laser radiation can be produced faster than any other relaxation process by a higher intensity light. Therefore, we have assumed

*¹Boeing Library of Mathematical Routines

it is 100 times faster than the biggest rate constant in the system.

Figure 3 shows the variation of the population fractions divided by their degeneracies of the levels with the nondimensional time, t' for the mixture $5\%CO_2 + 70\%N_2 + 25\%He$ and $Tv/T = 15$. The population fractions of the levels $CO_2(01^10)$, $CO_2(02^00)$ and $N_2(v=0)$ increase while the levels $CO_2(00^00)$, $CO_2(00^01)$ and $N_2(v=1)$ eventually decrease with t' up to a quasi-steady-state condition ($t'=5$). At $t'=5.02$, however, just after the laser has been turned on, the populations (particularly of the levels $CO_2(00^01)$ and $CO_2(02^00)$) are affected strongly; the levels $CO_2(00^01)$ and $CO_2(02^00)$ are bleached immediately. There becomes the possibility of obtaining a population inversion between the levels $CO_2(02^00)$ and $CO_2(01^10)$ because their relaxation time is much slower than the radiative relaxation time of $CO_2(00^01)$ and $CO_2(02^00)$ transition. These curves have the same trends and almost the same characteristics for the other conditions.

Figure 4 shows the variation of the population fraction over degeneracy versus the energy of the level for the mixture $5\%CO_2 + 70\%N_2 + 25\%He$ and $Tv/T = 10$ at $t'=5$. The level $CO_2(00^01)$ is characterized by the vibrational temperature Tv (solid straight line). The levels $CO_2(01^10)$, $CO_2(02^00)$, $CO_2(03^10)$, and $CO_2(04^00)$, however, are characterized by the translational temperature, T (dashed line). Because of exclusion of (V-V) transitions, this line has a slightly broken behavior rather than being straight. We note that the mixed modes (for example $CO_2(11^10)$, $CO_2(021)$ etc.) have been spread in the region between these two lines. It can be easily seen that we can never get population inversion between the levels $CO_2(02^00)$ and

CO₂(01¹0) unless with the lasing action at 10.6μ.

Figure 5 shows the variation of the gain coefficients, α (both at 10.6μ and 16.18μ) with T_v/T for a fixed He-concentration of 25% and with the ratio of CO₂ to N₂ as a variable. Higher CO₂ to N₂ ratios and higher vibrational to translational temperature ratios give higher gain. At $T_v/T = 7.5$, which corresponds to $T = 400^\circ\text{K}$, no 16.18μ gain has been predicted. Calculations have also shown that the gain at 10.6μ is higher than the gain at 16.18μ at these same conditions. The curves almost have straight line trends.

Figure 6 shows the variation of α with $X_{\text{CO}_2}/X_{\text{N}_2}$ for a fixed He-concentration (25%) and with translational temperature as a parameter ($T = 200, 300$ and 400°K). This figure supports the conclusion drawn in fig. 5. It is shown that higher CO₂ concentrations give higher radiation (or absorption) due to the higher density of CO₂ particles.

Figure 7 shows the effects of the mole fraction of He on the 16.18μ gain at fixed $X_{\text{CO}_2}/X_{\text{N}_2} (= 1/14)$ and $T = 300^\circ\text{K}$. Higher He-concentrations (up to 10%) increase the gain very fast; but for fractions higher than 10%, they decrease the gain slowly. At zero He-concentration, no gain has been predicted.

POPULATION FRACTIONS OF THE LEVELS / DEGENERACY, x_n/g_n

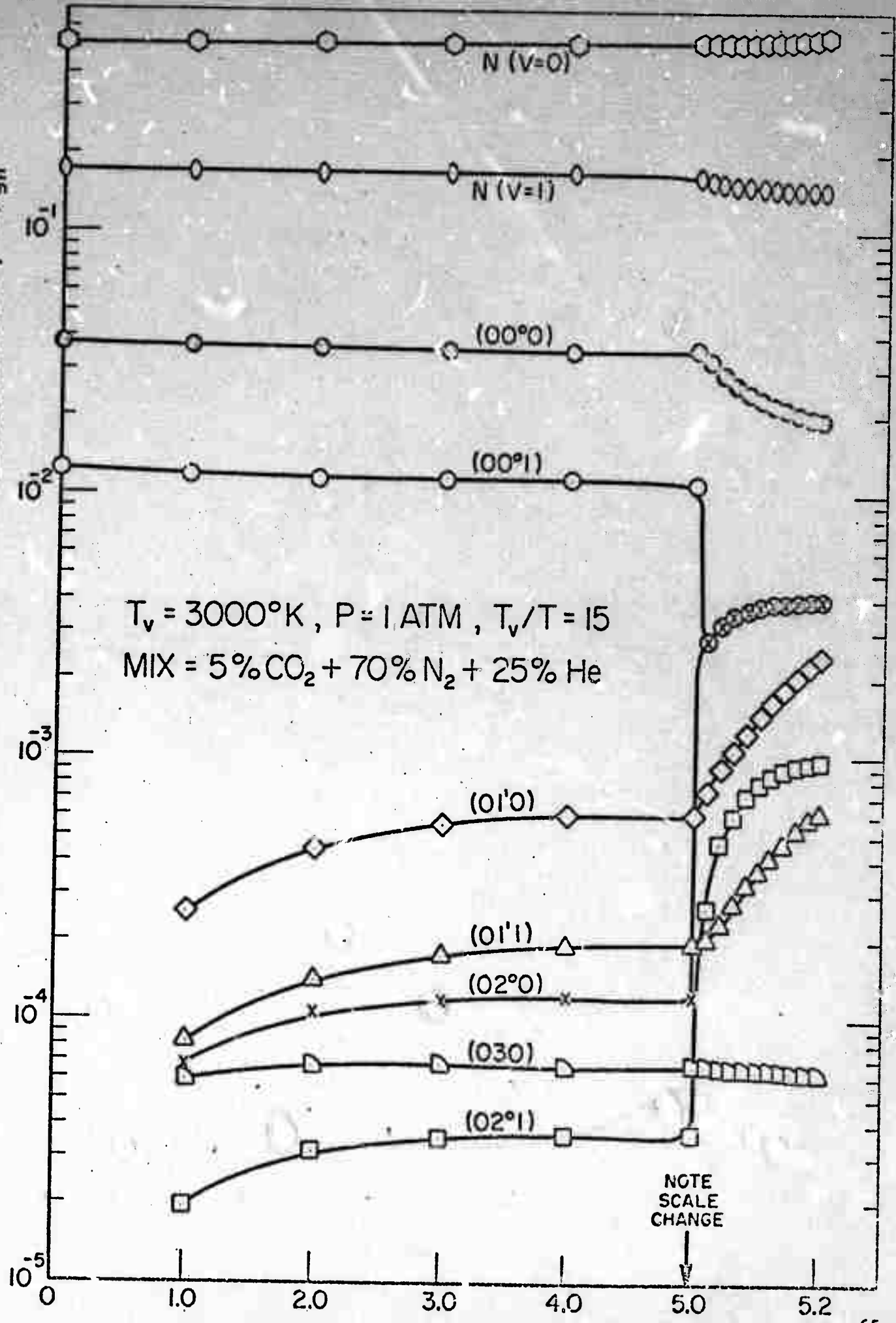


FIGURE 3

TIME t' ($t' = t \sum k_n^M M$)

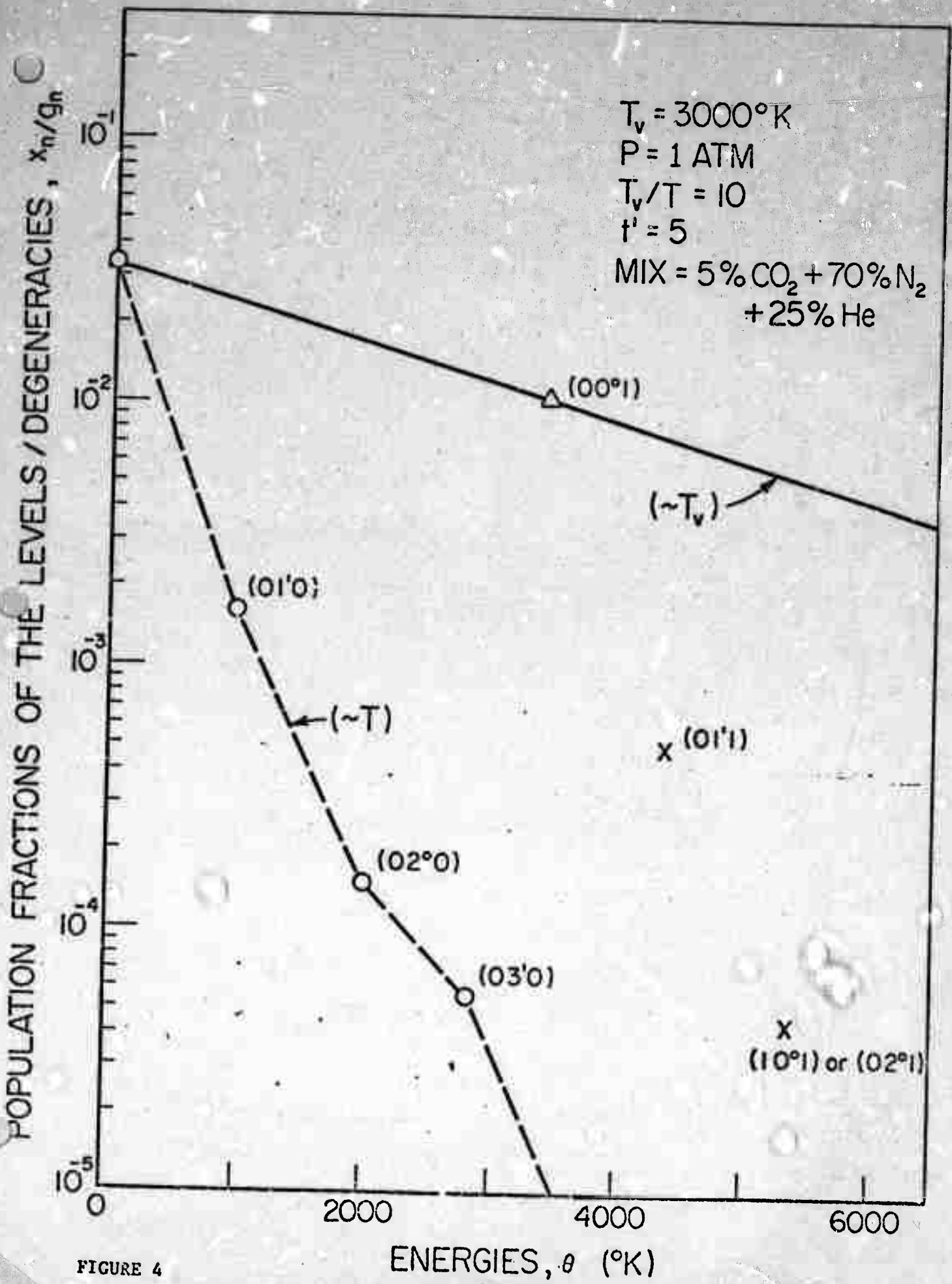


FIGURE 4

ENERGIES, θ ($^\circ\text{K}$)

TABLE - II

P = 1 ATM.

 $T_v = 3000^\circ\text{K}$

MIXTURE	T_v/T	GAIN COEFFICIENT, α (m^{-1})	
		$\text{CO}_2(02^00) - \text{CO}_2(01^10)$ $\lambda = 16.18\mu$	$\text{CO}_2(00^01) - \text{CO}_2(10^00)$ $\lambda = 10.6\mu$
5% CO_2	15	4.57	5.21
70% N_2	10	0.957	3.32
25%He	7.5	-0.816	2.35
2.5% CO_2	15	2.396	2.716
72.5% N_2	10	0.557	1.697
25%He	7.5	-0.413	1.12
1% CO_2	15	1.008	1.1
74% N_2	10	0.242	0.689
25%He	7.5	-0.1603	0.477

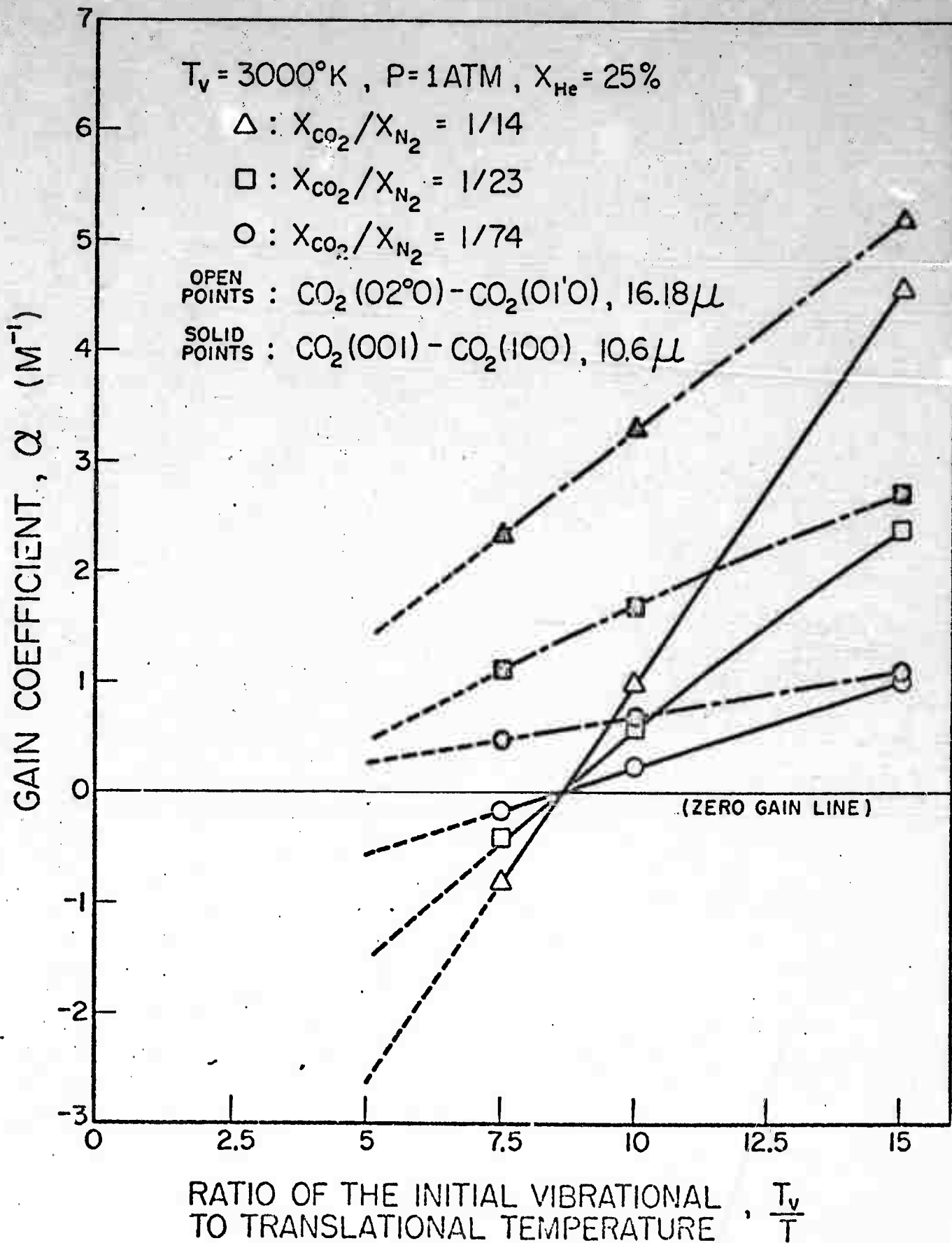


FIGURE 5. VARIATION OF GAIN COEFFICIENT WITH T_v/T

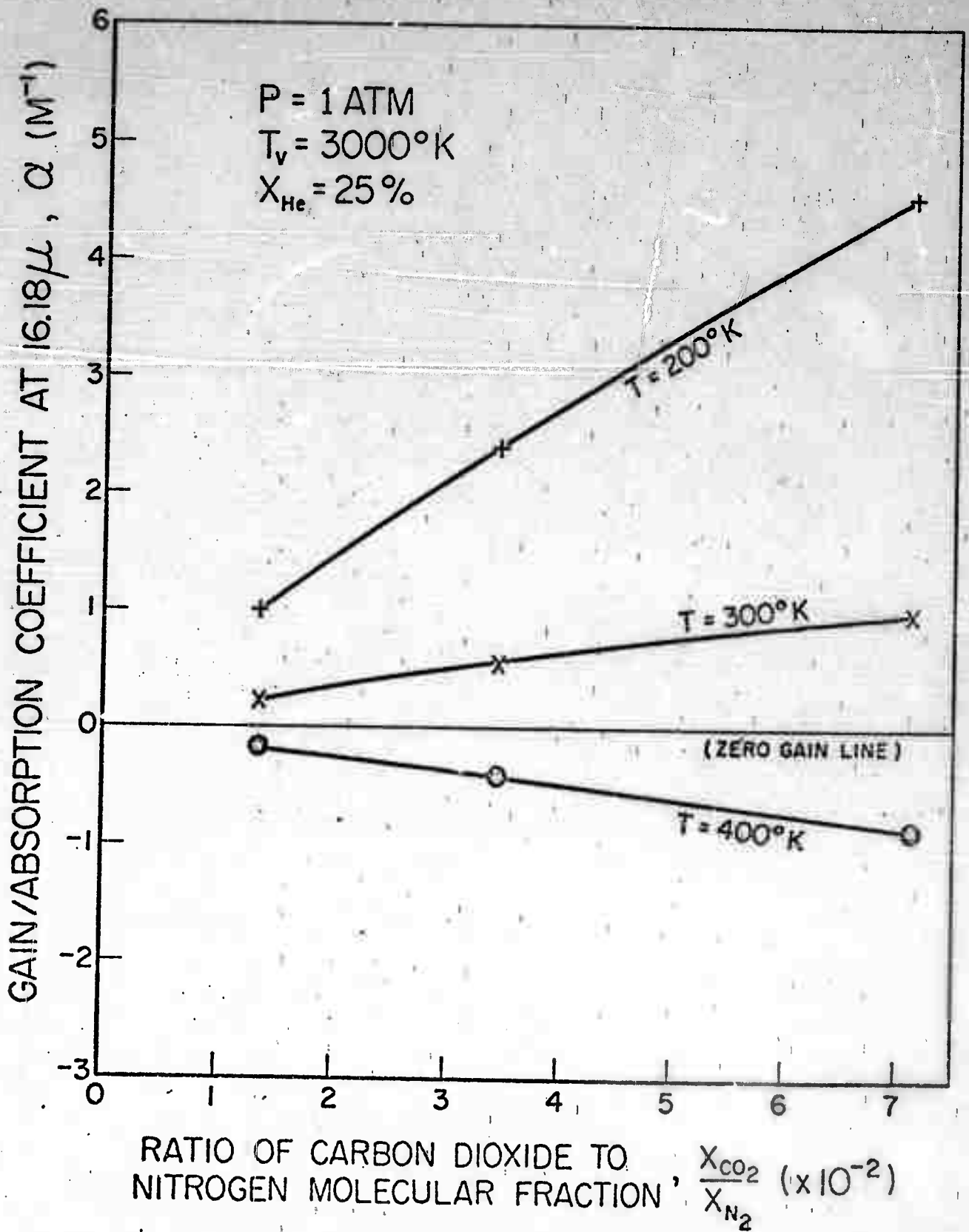


FIGURE 6. VARIATION OF α AT 16.18μ WITH $\frac{X_{\text{CO}_2}}{X_{\text{N}_2}}$

TABLE - III

$$X_{\text{CO}_2} / X_{\text{N}_2} = 1/14, \quad P = 1 \text{ ATM.}$$

$$T = 300^\circ\text{K}$$

$$T_v = 3000^\circ\text{K}$$

MIXTURE	MOLE FRACTION	GAIN COEF., $\alpha(\text{m}^{-1})$
	of He, % by volume	$\lambda = 16.18\mu$
6.65%CO ₂ + 93.35%N ₂	0	-2.39
6.35%CO ₂ + 88.66%N ₂ + 5%He	5	1.248
6%CO ₂ + 84%N ₂ + 10%He	10	1.35
5.665%CO ₂ + 79.335%N ₂ + 15%He	15	1.279
5%CO ₂ + 70%N ₂ + 25%He	25	0.957
4%CO ₂ + 56%N ₂ + 40%He	40	0.856
2.5%CO ₂ + 35%N ₂ + 62.5%He	62.5	0.514

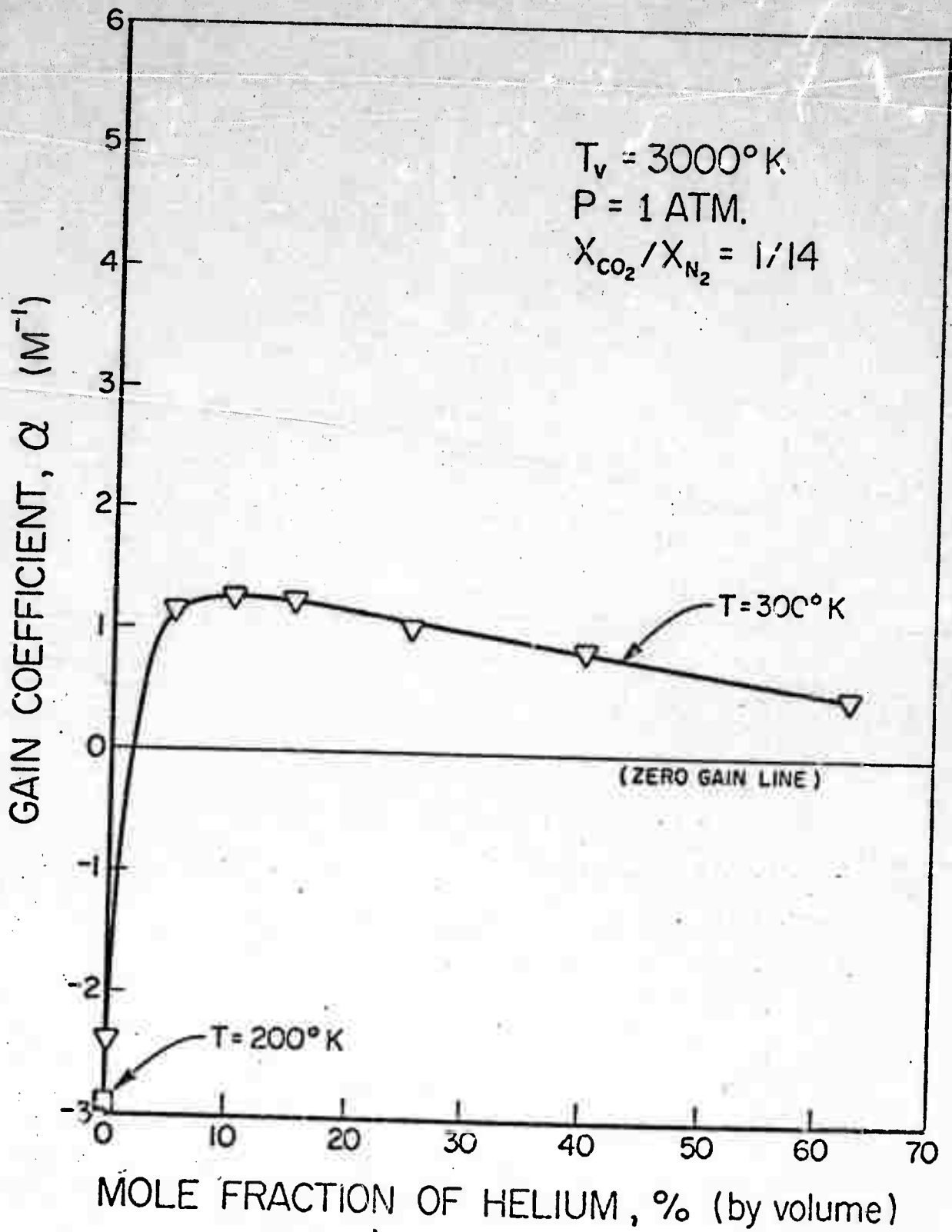
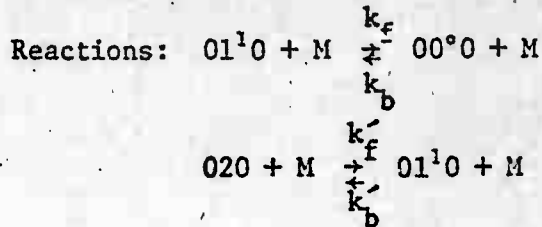
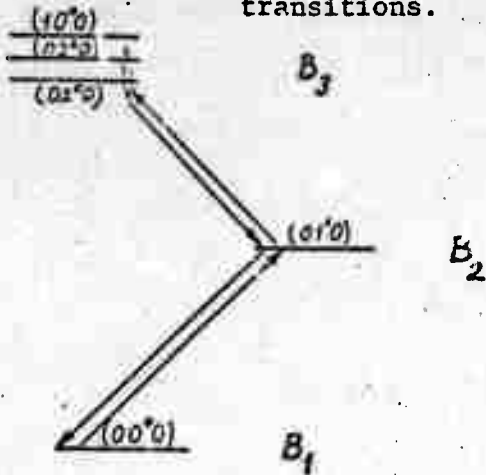


FIGURE 7. EFFECT OF He CONCENTRATION ON GAIN AT 16.18μ

ADDENDUM

Master Vibrational Relaxation Equations:

Consider the level $\text{CO}_2(01^10)$. It has 2 gains and 2 losses in (T-V) transitions.



$M = \text{CO}_2(01^10), \text{CO}_2(02^0), \text{CO}_2(10^0), \text{etc.}$

Then

$$\begin{aligned} \frac{dN_2}{dt}_{T-V} = & \left(-k'_{f_{1 \rightarrow 0}} N_2 N_2 + k_{b_{0 \rightarrow 1}} N_1 N_2 \right) + \left(k_{f_{2 \rightarrow 1}} \frac{3}{4} N_3 N_2 - k_{b_{1 \rightarrow 2}} N_2 N_2 \right) \\ & + \left(-k'_{f_{1 \rightarrow 0}} N_2 \frac{3}{4} N_3 + k_{b_{0 \rightarrow 1}} N_1 \frac{2}{3} N_3 \right) + \left(k_{f_{2 \rightarrow 1}} \frac{3}{4} N_3 \frac{2}{3} N_3 - k_{b_{1 \rightarrow 2}} N_2 \frac{3}{4} N_3 \right) \\ & + \left(-k'_{f_{1 \rightarrow 0}} N_2 \frac{2}{3} N_4 + k_{b_{0 \rightarrow 1}} N_1 \frac{2}{3} N_4 \right) + \left(k_{f_{2 \rightarrow 1}} \frac{3}{4} N_3 \frac{2}{3} N_4 - k_{b_{1 \rightarrow 2}} N_2 \frac{2}{3} N_4 \right) \\ & + \dots \\ & + \dots \\ & + \left(-k'_{f_{1 \rightarrow 0}} N_2 N_{25} + k_{b_{0 \rightarrow 1}} N_1 N_{25} \right) + \left(k_{f_{2 \rightarrow 1}} \frac{3}{4} N_3 N_{25} - k_{b_{1 \rightarrow 2}} N_2 N_{25} \right) \\ & + \left(-k'_{f_{1 \rightarrow 0}} N_2 N_{N(v=0)} + k_{b_{0 \rightarrow 1}} N_1 N_{N(v=0)} \right) + \left(k_{f_{2 \rightarrow 1}} \frac{3}{4} N_3 N_{N(v=0)} - k_{b_{1 \rightarrow 2}} N_2 N_{N(v=0)} \right) \\ & + \left(-k'_{f_{1 \rightarrow 0}} N_2 N_{N(v=1)} + k_{b_{0 \rightarrow 1}} N_1 N_{N(v=1)} \right) + \left(k_{f_{2 \rightarrow 1}} \frac{3}{4} N_3 N_{N(v=1)} - k_{b_{1 \rightarrow 2}} N_2 N_{N(v=1)} \right) \end{aligned}$$

Or,

$$\begin{aligned} \frac{dN_2}{dt} \Big|_{T-V} = & \left(-k_{f_{1 \rightarrow 0}} N_2 \sum_{i=1}^{25} N_i + k_{b_{0 \rightarrow 1}} N_1 \sum_{i=1}^{25} N_i \right) + \left(k_{f_{2 \rightarrow 1}} \frac{3}{4} N_3 \sum_{i=1}^{25} N_i - k_{b_{1 \rightarrow 2}} N_2 \sum_{i=1}^{25} N_i \right) \\ & + \left(-k'_{f_{1 \rightarrow 0}} N_2 \sum_{j=1}^2 N_{N_j} + k'_{b_{0 \rightarrow 1}} N_1 \sum_{j=1}^2 N_{N_j} \right) + \left(k'_{f_{2 \rightarrow 1}} \frac{3}{4} N_3 \sum_{j=1}^2 N_{N_j} - k'_{b_{1 \rightarrow 2}} N_2 \sum_{j=1}^2 N_{N_j} \right) \end{aligned}$$

Since $\sum_{i=1}^{25} N_i = N_{CO_2}$

$\sum_{j=1}^2 N_{N_j} = N_{N_2}$

and

$$k_{f_{2 \rightarrow 1}} = 2 k_{f_{1 \rightarrow 0}} \quad , \quad k_{f_{3 \rightarrow 2}} = 3 k_{f_{1 \rightarrow 0}} \quad , \quad \text{etc.}$$

and

$$k_e = \frac{k_{f_{1 \rightarrow 0}}}{k_{b_{0 \rightarrow 1}}} = \frac{N_{000} N_{01'0}}{(N_{01'0})^2} = \frac{N_{000}}{N_{01'0}} = \frac{N_{00'0}}{2 \cdot N_{00'0} \cdot e^{-\theta/T}} = \frac{1}{2} e^{\theta/T}$$

etc.

from the following relations

$$k_{i \rightarrow i-1} = i k_{1 \rightarrow 0} \quad , \quad k_{i+1 \rightarrow i} = (i+1) k_{1 \rightarrow 0}$$

$$k_{i-1 \rightarrow i} = i k_{1 \rightarrow 0} e^{-\theta_i/T} \quad , \quad k_{i \rightarrow i+1} = (i+1) k_{1 \rightarrow 0} e^{-\theta_i/T}$$

Now, introducing the population fractions of the boxes (B_1, B_2, \dots see Fig. 2),

i.e., $X_1 \left(\equiv \frac{N_1}{N} \right)$, finally we have

$$\frac{dX_2}{dt} \Big|_{T-V} = \sum k_{f_{1 \rightarrow 0}}^M \left[(2 \exp(-\theta/T) X_1 - X_2) + (3/2 X_3 - 3 \exp(-\theta/T) X_2) \right]$$

Likewise, doing the same type analysis for each box and for each relaxation process (i.e., T-V, Radiations, Special transitions), the complete set of master relaxations equations, used at the computer, are given as:

THE SET OF MASTER VIBRATIONAL RELAXATION EQUATIONS:

$$\frac{dX_1}{dt}_T = \sum k_{f_1 \rightarrow 0}^M M \left[X_2 - 2 \exp(-\theta/T) X_1 \right] + k_f N (X_5 X_{11} - X_1 X_{10}) + K_4 I_4 (X_2 - X_1)$$

$$\frac{dX_2}{dt}_T = \sum k_{f_1 \rightarrow 0}^M M \left[(2 \exp(-\theta/T) X_1 - X_2) + (3/2 X_3 - 3 \exp(-\theta/T) X_2) \right]$$

$$+ k_f N (X_7 X_{11} - X_2 X_{10}) + K_2 I_2 (1/4 X_3 - X_2) + K_3 I_3 (3/4 X_3 - X_2)$$

$$+ K_4 I_4 (X_1 - X_2)$$

$$\frac{dX_3}{dt}_T = \sum k_{f_1 \rightarrow 0}^M M \left[(3 \exp(-\theta/T) X_2 - 3/2 X_3) + (7/3 X_4 - 7/2 \exp(-\theta/T) X_3) \right]$$

$$+ k_f N \left[3/4 (X_9 X_{11} - X_3 X_{10}) \right] + (K_L I_L + K_1 I_1) (X_5 - 1/4 X_3)$$

$$+ K_2 I_2 (X_2 - 1/4 X_3) + (X_2 - 3/4 X_3) K_3 I_3$$

$$\frac{dX_4}{dt}_T = \sum k_{f_1 \rightarrow 0}^M M \left[(7/2 \exp(-\theta/T) X_3 - 7/3 X_4) + (26/3 X_6 - 13/3 \exp(-\theta/T) X_4) \right]$$

$$+ \sum k_{f_{001 \rightarrow 030}}^M M \left[X_5 - 1/6 \exp(-\bar{\theta}/T) X_4 \right] + K_L I_L (X_7 - 1/3 X_4)$$

$$\frac{dX_5}{dt}_T = \sum k_{f_1 \rightarrow 0}^M M \left[X_7 - 2 \exp(-\theta/T) X_5 \right] + k_f N (X_1 X_{10} - X_5 X_{11})$$

$$+ \sum k_{f_{001 \rightarrow 030}}^M M \left[1/6 \exp(-\bar{\theta}/T) X_4 - X_5 \right]$$

$$+ (K_L I_L + K_1 I_1) (1/4 X_3 - X_5)$$

$$\begin{aligned} \frac{dX_6}{dt} \Big|_T &= \sum_{k_{f_1 \rightarrow 0}} k_{f_1 \rightarrow 0}^M M \left[\frac{13}{3} \exp(-\theta/T) X_4 - \frac{26}{9} X_6 \right] + \left(\frac{11}{3} X_8 - \frac{44}{9} \exp(-\theta/T) X_6 \right) \\ &+ \sum_{k_{f_{001 \rightarrow 030}}} k_{f_{001 \rightarrow 030}}^M M \left[X_7 - \frac{2}{9} \exp(-\bar{\theta}/T) X_6 \right] + K_L I_L \left(\frac{3}{4} X_9 - \frac{1}{3} X_6 \right) \end{aligned}$$

$$\begin{aligned} \frac{dX_7}{dt} \Big|_T &= \sum_{k_{f_1 \rightarrow 0}} k_{f_1 \rightarrow 0}^M M \left[\left(2 \exp(-\theta/T) X_5 - X_7 \right) + \left(\frac{3}{2} X_9 - 3 \exp(-\theta/T) X_7 \right) \right] \\ &+ k_f N (X_2 X_{10} - X_7 X_{11}) + \sum_{k_{f_{001 \rightarrow 030}}} k_{f_{001 \rightarrow 030}}^M M \left[\frac{2}{9} \exp(-\bar{\theta}/T) X_6 - X_7 \right] \\ &+ K_L I_L \left(\frac{1}{3} X_4 - X_7 \right) \end{aligned}$$

$$\frac{dX_8}{dt} \Big|_T = \sum_{k_{f_1 \rightarrow 0}} k_{f_1 \rightarrow 0}^M M \left[\left(\frac{44}{9} \exp(-\theta/T) X_6 - \frac{11}{3} X_8 \right) \right] + \sum_{k_{f_{001 \rightarrow 030}}} k_{f_{001 \rightarrow 030}}^M M \left[X_9 - \frac{1}{3} \exp(-\bar{\theta}/T) X_8 \right]$$

$$\begin{aligned} \frac{dX_9}{dt} \Big|_T &= \sum_{k_{f_1 \rightarrow 0}} k_{f_1 \rightarrow 0}^M M \left[\left(3 \exp(-\theta/T) X_7 - \frac{3}{2} X_9 \right) \right] + k_f N \left[\frac{3}{4} (X_3 X_{10} - X_9 X_{11}) \right] \\ &+ \sum_{k_{f_{001 \rightarrow 030}}} k_{f_{001 \rightarrow 030}}^M M \left[\frac{1}{3} \exp(-\bar{\theta}/T) X_8 - X_9 \right] + K_L I_L \left(\frac{1}{3} X_6 - \frac{3}{4} X_9 \right) \end{aligned}$$

$$\frac{dX_{10}}{dt} \Big|_T = \sum_{k_{f_1 \rightarrow 0} (N_2)} k_{f_1 \rightarrow 0}^M M (X_{11} - X_{10}) + k_f N \left[(X_5 + X_7 + \frac{3}{4} X_9) X_{11} - (X_1 + X_2 + \frac{3}{4} X_3) X_{10} \right]$$

$$\frac{dX_{11}}{dt} \Big|_T = \sum_{k_{f_1 \rightarrow 0} (N_2)} k_{f_1 \rightarrow 0}^M M (X_{10} - X_{11}) + k_f N \left[(X_1 + X_2 + \frac{3}{4} X_3) X_{10} - (X_5 + X_7 + \frac{3}{4} X_9) X_{11} \right]$$

WHERE X_i 's ARE THE POPULATION FRACTIONS OF THE BOXES IN FIG. 2.

AT THE EQUILIBRIUM:

$$\sum_{i=1}^{11} \frac{dX_i}{dt} \Big|_T \equiv 0$$

where

$$\sum k_{f_{1 \rightarrow 0}}^M = k_{f_{1 \rightarrow 0}}^{CO_2} N_{CO_2} + k_{f_{1 \rightarrow 0}}^{N_2} N_{N_2} + k_{f_{1 \rightarrow 0}}^{He} N_{He}$$

$$\sum k_{f_{1 \rightarrow 0}}^M (N_2) = k_{f_{1 \rightarrow 0}}^{CO_2} (N_2) N_{CO_2} + k_{f_{1 \rightarrow 0}}^{N_2} (N_2) N_{N_2} + k_{f_{1 \rightarrow 0}}^{He} (N_2) N_{He}$$

and they are related to (T-V) transitions.

$k_{f_{1 \rightarrow 0}}^{CO_2}$ is the rate constant that a CO_2 -molecule in quantum level (01^10) will suffer a collision with another CO_2 -molecule and make a transition to ground level (00^00) per second.

$k_{f_{1 \rightarrow 0}}^{N_2}$ is the rate constant of the collision a CO_2 -molecule with a N_2 -molecule.

$k_{f_{1 \rightarrow 0}}^{CO_2} (N_2)$ is the rate constant that a N_2 -molecule in quantum level $(v=1)$ will suffer a collision with a CO_2 -molecule and make a transition to ground level $(v=0)$ per second.

Likewise for the others.

N_{CO_2} , N_{N_2} , N_{He} are the total number of particles of CO_2 , N_2 , He, respectively.
and

$$\sum k_{f_{001-030}}^M = k_{f_{001-030}}^{CO_2} N_{CO_2} + k_{f_{001-030}}^{N_2} N_{N_2} + k_{f_{001-030}}^{He} N_{He}$$

and they are related to SP_2 transitions.

$k_{f_{001-030}}^{CO_2}$ is the rate constant that a CO_2 -molecule in quantum level (001) will suffer a collision with another CO_2 -molecule and make a transition to level (030) per second.

Likewise for the others.

and

$k_f \equiv k_{f_{000-001}} \equiv k_{f_{010-011}} \equiv k_{f_{020-021}}$ is related to SP_1 transitions.

I 's are the intensities of the radiations (refer to fig. 2).

$\Theta \equiv \Theta(01^10) = 667.3\text{cm}^{-1}$: The energy of the level $\text{CO}_2(01^10)$

$\bar{\Theta} \equiv [\Theta(001) - \Theta(030)] = 380\text{cm}^{-1}$: the energy difference between the levels $\text{CO}_2(001)$ and $\text{CO}_2(030)$.

We note that in our computer program these equations have been divided through $\Sigma k_{f_1 \rightarrow 0}^M M$, and the nondimensional time, t' has been defined as:

$$t' = t \Sigma k_{f_1 \rightarrow 0}^M M$$

REFERENCES

1. Hertzberg, A., Johnston, E. W. and Ahlstrom, H. G., "Photon Generators and Engines for Laser Power Transmission," AIAA Paper, No. 71-106, Jan. 1971.
2. "Second Conference on the Laser", Annals of the New York Academy of Sciences, Vol. 168, Art. 3, Feb. 1970.
3. Rubin, R. J. and Shuler, K. E., "Relaxation of Vibrational Nonequilibrium Distributions. I. Collisional Relaxation of a System of Harmonic Oscillators," Journal of Chemical Physics, Vol. 25, No. 1, July 1956, pp. 59-67.
4. Rubin, R. J. and Shuler, K.E., "Relaxation of Vibrational Nonequilibrium Distributions. II. The Effects of the Collisional Transition Probabilities on the Relaxation Behavior," Journal of Chemical Physics, Vol. 25, No. 1, July 1956, pp. 68-74.
5. Rubin, R. J. and Shuler, K. E., "On the Relaxation of Vibrational Nonequilibrium Distributions. III. The Effects of Radiative Transitions on the Relaxation Behavior," Journal of Chemical Physics, Vol. 26, No. 1, Jan. 1952, pp. 137-142.
6. Montroll, E. W. and Shuler, K. E., "Studies in Nonequilibrium Rate Processes. I. The Relaxation of a System of Harmonic Oscillators," Journal of Chemical Physics, Vol. 26, No. 3, March 1957, pp. 454-464.
7. Basov, N. G., Oraevskii, N. G., and Shcheglov, V. A., "Production of a Population Inversion in Molecules of a Working Gas Mixed with a Thermally Excited Auxiliary Gas," Soviet Physics-Technical Physics, Vol. 15, No. 1, July, 1970, pp. 126-130.

8. Tychinskii, V. P., "Powerful Gas Lasers", Soviet Physics Uspekhi, Vol. 10, No. 2, Sept.-Oct. 1967, pp. 131-152.
9. Gerry, E. T., "Gas Dynamic Lasers," Invited paper presented in session GA of the APS Washington Meeting, 29 April 1970.
10. Tourin, R. H. and Henry, P. M. "Infrared Spectral Emissivities and Internal Energy Distribution of Carbon Dioxide at High Temperatures. Part I. Internal Energy Calculations," AD-313969, Dec. 1958, The Warner & Swasey Company Control Instrument Division 34W. 33 St., New York 1, New York.
11. Private communication with Dr. W. H. Christiansen, University of Washington.
12. Rapp, D., "Interchange of Vibrational Energy Between Molecules in Collisions," Journal of Chemical Physics, Vol. 43, 1965, pp. 316-317.
13. Meunier, B. M., "Viscous Flow Effects on CO₂-Laser Gain Measurements," M.S. Thesis, University of Washington, 1970.
14. Statz, H. Tang, C. L., and Koster, G. F., "Transition Probabilities Between Laser States in Carbon Dioxide," Journal of Applied Physics, Vol. 37, No. 11, Oct. 1966, pp. 4278-4284.
15. Patel, C.K.N., "Continuous-Wave Laser Action on Vibrational-Rotational Transitions of CO," Physical Review, Vol. 136 No. 5A, Nov. 1964, pp. A1187-A1193
16. Taylor, R. L. and Bitterman, S., "Survey of Vibrational Relaxation Data for Processes Important in the CO₂-N₂ Laser System, Review of Modern Physics, Vol. 41, No. 1, Jan. 1969, pp. 26-47.

APPENDIX C

Four Temperature Computer Program

Introduction:

A new and simplified four temperature model computer program was developed to explore the total pressure losses of various geometries and mixtures and also to support gain measurements of both the high temperature studies and the supersonic nozzle development.

The new program uses an approach analogous to the previous two temperature program (1), but it includes improvements other than using four temperatures instead of two. As before, the program calculates the parameters (p, T, gain, etc.) along any given streamtube. In addition, the new program includes Doppler broadening effects on the line center gain coefficient, entropy production, and a calculation of the total pressure and temperature.

It avoids using γ ($= c_p/c_v$) in the flow equations and, with four temperatures, has a more realistic lasing routine. The effects of small percentages of H_2O , CO , O_2 , and Ar can also be included in this new program.

Flow Equations:

A set of flow equations has been derived which are more practical for this application. A necessary result of considering vibrational energy is that γ , the specific heat ratio, varies. To avoid using γ , there has been defined a variable B to replace M, the Mach number, where $B^2 = \frac{u^2}{RT} = \gamma M^2$.

The quasi-one-dimensional-inviscid flow equations were developed in terms of B and in a stepwise formulation for computer application. Stepwise area ratio, $\frac{A_2}{A_1}$, is the only "known" of the equations. The momentum equation includes the wall pressure term from area change, $(\frac{P_1 + P_2}{2})(A_2 - A_1)$. The energy equation is for translation and rotation only, since Q is calculated from the vibrational energy relaxation equations.

$$\text{Continuity: } \frac{P_2}{P_1} = \frac{A_1 B_1}{A_2 B_2} \sqrt{\frac{T_2}{T_1}} \quad (1)$$

$$\text{Momentum: } \frac{P_2}{P_1} = (1 + \frac{A_2}{A_1} + 2 B_1^2) / (1 + \frac{A_2}{A_1} + 2 \frac{A_2}{A_1} B_2^2) \quad (2)$$

$$\text{Energy: } \left\{ \frac{C}{R} \right\}_{T,R} + \frac{1}{2} B_1^2 \cdot T_1 + Q = \left\{ \frac{C}{R} \right\}_{T,R} + \frac{1}{2} B_2^2 \cdot T_2 \quad (3)$$

where $\left\{ \frac{C}{R} \right\}_{T,R}$ includes only the translational and rotational degrees of freedom, and Q is the heat transferred into translation and rotation from vibration.

Vibrational Relaxation Equations:

The vibrational relaxation equations were written for four temperatures: T, translational-rotational; T_L , the lower modes of CO_2 (symmetric stretch (1) and bending (2)); T_U , the upper mode of CO_2 (asymmetric stretch); and T_N , the N_2 vibrational temperature (see Figure (1)). The corresponding energies in the modes are $E_L (=E_1 + 2E_2)$, E_U and E_N . The assumption of equilibrium within a mode is made, and the bending mode is assumed to be in equilibrium with the symmetric stretch mode. There is no assumption that T_L is "nearly in equilibrium" with T.

In order to use the technique of Stollery and Smith⁽²⁾, the relaxation equations were derived into the Bethe-Teller form:

$$\frac{dE}{dt} = \frac{1}{\tau} \{E^* - E\}$$

where E is the vibrational energy, E^* is the equilibrium vibrational energy, and τ the relaxation time (a function of p, T). In order to do this without approximations, some slowly varying quantities, all nearly unity, were introduced (Z_A, Z_B, Z_C). The relaxation equations became:

$$\frac{dE_L}{dt} = \frac{2}{\tau_L} \{E^*_2 - E_2\} - \frac{(\Theta_1 + \Theta_2)}{\Theta_3} Z_A \frac{1}{\tau_U} \{E^*_U - Z_B E_U\} \quad (4)$$

$$\frac{dE_U}{dt} = Z_A \frac{1}{\tau_U} \{E^*_U - Z_B E_U\} + \frac{1}{\tau_N} \left\{ \frac{\psi_{\text{CO}_2}}{\psi_{\text{N}_2}} Z_C E_N - E_U \right\} \quad (5)$$

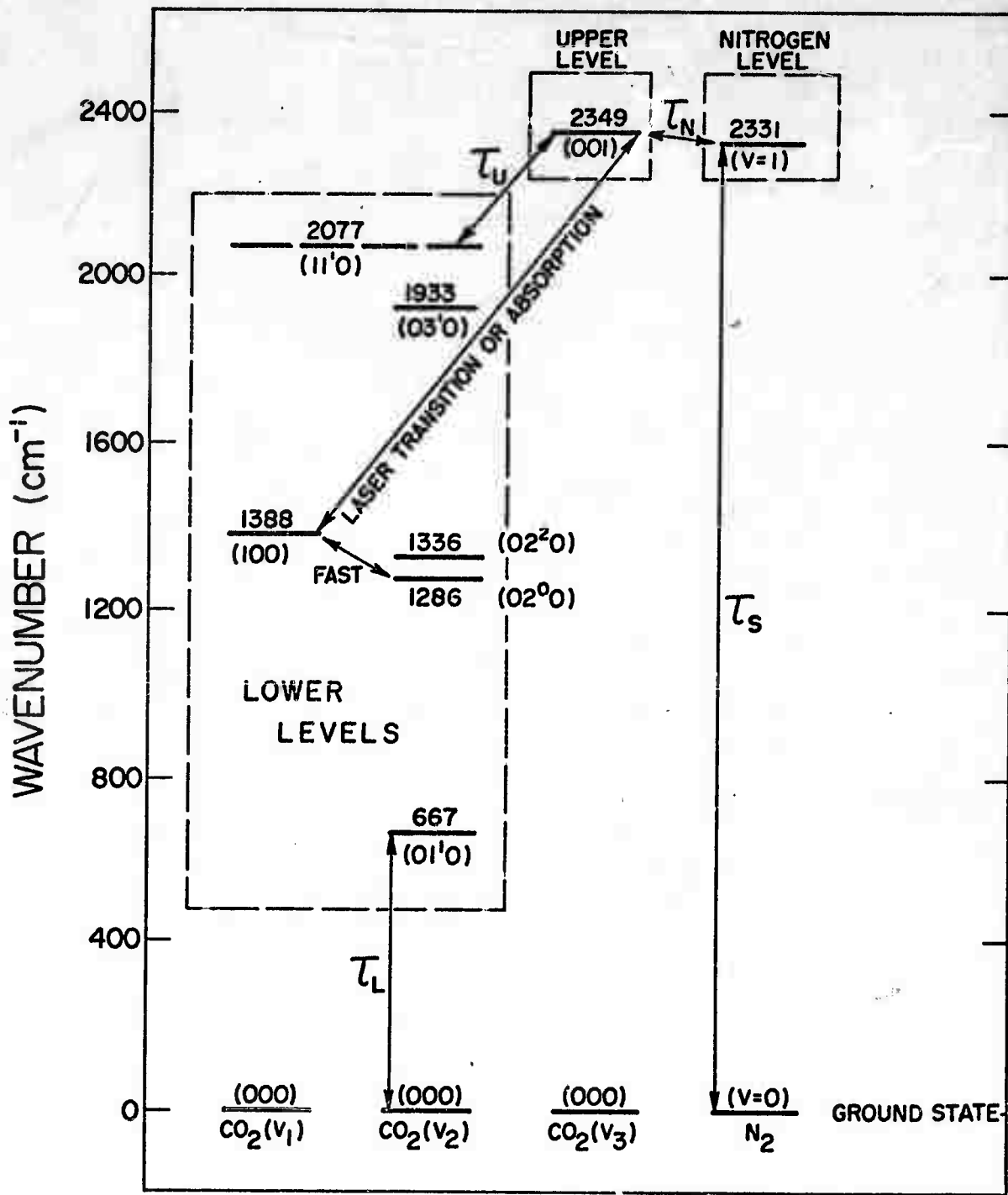


Figure 1. Vibrational Energy-Level Diagram for CO₂ - N₂ System.

$$\frac{dE_N}{dt} = \frac{1}{\tau_N} \frac{\theta_N}{\theta_3} \{E_U - \frac{\psi_{CO_2}}{\psi_{N_2}} Z_C E_N\} + \frac{1}{\tau_2} (E_N^* - E_N) \quad (6)$$

where

$$Z_A = \frac{E_1}{E_1^*} \cdot \frac{E_2}{E_2^*}$$

$$Z_B = \frac{\exp\left(\frac{\theta_3}{T} + (\theta_1 + \theta_2) \left(\frac{1}{T_L} - \frac{1}{T}\right)\right) - 1}{\exp\left(\frac{\theta_3}{T}\right) - 1}$$

$$Z_C = \frac{\theta_3}{\theta_N} Z_D + \frac{E_U}{\psi_{CO_2} \theta_N} (Z_D - 1) \quad ; \quad Z_D = \exp\left(\frac{\theta_N - \theta_3}{T}\right)$$

$$E_L = E_1 + 2E_2$$

$$E_1 = \frac{\psi_{CO_2} \theta_1}{\exp\left(\frac{\theta_1}{T_L}\right) - 1} \quad ; \quad E_2(T_L), E_U(T_U), E_N(T_N) \text{ are analogous}$$

ψ_{CO_2}, ψ_{N_2} = mole fractions

$\theta_1, \theta_2, \theta_3, \theta_N$ = characteristic vibrational temperatures

NOTE: $Q = E_{L_1} + E_{U_1} + E_{N_1} - (E_{L_2} + E_{U_2} + E_{N_2})$

The first term in (4) represents the deactivation of the lower levels to the ground state. The last term in (4) and the first in (5) represent the transfer of energy from the upper level to the lower levels. The last term in (5) and the first of (6) represent the coupling of the upper level and the N_2 vibration. The last term of (7) is the slow deactivation of the N_2 vibration directly to the ground state.

To solve the relaxation equations, the equations have been written in difference equation form suggested by Stollery and Smith⁽²⁾. Note that (5) and (6) can be solved independently of (4). By solving for E_2 as a function of E_L , (4) is solved without iteration.

Lasing is presently accomplished by extracting all available energy in the CO₂ upper level, while appropriately raising the lower level energy until zero gain is reached. This corresponds to an infinite laser intensity.

Relaxation Time Equations:

The relaxation times τ_L , τ_N , τ_S , and $(\tau_U)_{H_2O}$ are from Taylor and Bitterman's⁽³⁾ data. The remaining τ_U are from the data of Rosser, Wood, and Gerry⁽⁴⁾. The $p\tau$ versus $T^{-1/3}$ equations are approximations to the best fit curves given and are in agreement with, and fit the data better than, those of Munjee⁽⁵⁾ and Anderson⁽⁶⁾.

The equation used to find the relaxation time of a gas mixture from its components is:

$$\frac{1}{p\tau} = \sum_{\text{all species}} \frac{\psi_{\text{species}}}{(p\tau)_{\text{species}}}$$

The curve fits for $p\tau_L$, in atm-sec:

300 - 460°K	$(p\tau_L)_{CO_2} = 2(10^{-6}) \exp(24T^{-1/3})$
	$(p\tau_L)_{N_2} = 9(10^{-7}) \exp(24.7T^{-1/3})$
	$(p\tau_L)_{He} = 9.34(10^{-8}) \exp(8.96T^{-1/3})$
460 - 2000°K	$(p\tau_L)_{CO_2} = 3.06(10^{-9}) \exp(56.1T^{-1/3})$
	$(p\tau_L)_{N_2} = 1.61(10^{-8}) \exp(55.8T^{-1/3})$
	$(p\tau_L)_{He} = 1.8(10^{-8}) \exp(21.6T^{-1/3})$
300 - 2000°K	$(p\tau_L)_{H_2O} = 1.04(10^{-5}) \exp(-55.5T^{-1/3})$

The curve fits for $p\tau_U$, in atm-sec:

300 - 380°K	$(p\tau_U)_{CO_2} = 2.04(10^{-6}) \exp(4.28T^{-1/3})$
380 - 2000°K	$(p\tau_U)_{CO_2} = 2.67(10^{-10}) \exp(68.9T^{-1/3})$
300 - 615°K	$(p\tau_U)_{N_2} = 6.75(10^{-8}) \exp(34.2T^{-1/3})$
615 - 2000°K	$(p\tau_U)_{N_2} = 4.3(10^{-12}) \exp(116.5T^{-1/3})$

$$300 - 2000^{\circ}\text{K} \quad (p\tau_u)_{\text{He}} = 1.5 (p\tau_u)_{\text{N}_2}$$

$$(p\tau_u)_{\text{H}_2\text{O}} = 2.74 (10^{-7}) \exp(-12.8T^{-1/3})$$

The curve fit for $p\tau_N$, in atm-sec:

$$300 - 1000^{\circ}\text{K} \quad (p\tau_N)_{\text{N}_2} = 1.4 (10^{-11}) T^{1.5}$$

$$1000 - 1400^{\circ}\text{K} \quad (p\tau_N)_{\text{N}_2} = 4.5 (10^{-7})$$

$$1400 - 2000^{\circ}\text{K} \quad (p\tau_N)_{\text{N}_2} = 3.5 (10^{-6}) \exp(-\frac{T}{670})$$

The curve fits for $p\tau_s$, in atm-sec:

$$300 - 2000^{\circ}\text{K} \quad (p\tau_s)_{\text{CO}_2} = (p\tau_s)_{\text{N}_2}$$

$$(p\tau_s)_{\text{N}_2} = 9.52 (10^{-17}) T \exp(278T^{-1/3})$$

$$(p\tau_s)_{\text{He}} = 2.88 (10^{-13}) T \exp(111T^{-1/3})$$

$$(p\tau_s)_{\text{H}_2\text{O}} = 7.6 (10^{-11}) \exp(88T^{-1/3})$$

For small fractions of CO, O₂ or Ar, a good guess is to use $(p\tau)_{\text{N}_2}$ in all cases.

Summary:

This four temperature CO₂-N₂ kinetics program is quite inexpensive, yet retains good accuracy (T within 10°K of the more costly programs). It also remains flexible and can handle any nozzle flow problem with vibrational relaxation. The program is being expanded to handle the effect of varying laser intensities. Vibration-vibration coupling of CO with CO₂ will be included when the data becomes available.

APPENDIX C

References

1. D. A. Russell, R. A. Tennant, and G. W. Butler, "Shock Tube Configuration for the Study of Population Inversion." Air Force Weapons Laboratory Technical Report #AFWL TR-71-15. March 1971.
2. J. L. Stollery and J. E. Smith, J. Fluid Mech. 13, 225(1962).
3. R. L. Taylor and S. Bitterman, Rev. Mod. Phys. 41, 26(1969).
4. W. A. Rosser, Jr., A. D. Wood, and E. T. Gerry, J. Chem. Phys. 50, 4996(1969).
5. S. A. Munjee, The Phys. of Fluids 15, 506(1972).
6. J. D. Anderson, R. P. Humphrey, J. S. Vamos, M. J. Plummer and R. E. Jensen, The Phys. of Fluids 14, 2620(1971).